Progress and Outlooks in Designing Photonic Biosensor for Virus Detection

Annisa Tsalsabila, Valentinus Dabur, Indra Budiarso, Shofarul Wustoni, Heng-chang Chen, Muhammad Birowosuto, Arie Wibowo, Shuwen Zeng

Progress and Outlooks in Designing Photonic Biosensor for Virus Detection

Annisa Tsalsabila[‖], *Valentinus A. Dabur*[‖], *Indra J. Budiarso, Shofarul Wustoni, Heng-Chang Chen, Muhammad D. Birowosuto, Arie Wibowo*[*], *and Shuwen Zeng*[*]

A. Tsalsabila
Doctoral program in Materials Science and Engineering, Faculty of Mechanical and Aerospace Engineering, Institut Teknologi Bandung, Jl. Ganesha 10, 40132 Bandung, Indonesia.

V. A. Dabur, I. J. Budiarso
Master program in Materials Science and Engineering, Faculty of Mechanical and Aerospace Engineering, Institut Teknologi Bandung, Jl. Ganesha 10, 40132 Bandung, Indonesia.

S. Wustoni
Biological and Environmental Science and Engineering Division, King Abdullah University of Science and Technology (KAUST), Thuwal, 23955-6900, Saudi Arabia.

H. C. Chen, M. D. Birowosuto
Łukasiewicz Research Network—PORT Polish Center for Technology Development, Stabłowicka 147, 54-066, Wrocław, Poland.

A. Wibowo
*Materials Science and Engineering, Faculty of Mechanical and Aerospace Engineering, Institut Teknologi Bandung, Jl. Ganesha 10, 40132 Bandung, Indonesia
**Research Center for Nanoscience and Nanotechnology, Institut Teknologi Bandung, Ganesha 10, Bandung 40132, West Java, Indonesia.
E-mail: ariewibowo@itb.ac.id

S. Zeng
Light, Nanomaterials & Nanotechnologies (L2n), CNRS-UMR7076, Université de Technologie de Troyes, 10000 Troyes, France.
Email: shuwen.zeng@cnrs.fr

[‖]contributed equally to this work

Keywords: biorecognition element, photonic biosensor, photonic materials, photonic methods, virus detection

Abstract:

The recent outbreak of SARS-CoV-2 highlights the critical need for rapid, sensitive, and accurate virus detection methods to prevent and manage pandemics. Among the available sensing methods, photonic biosensors have emerged as a forefront technology, characterized by their high sensitivity, minimal analyte requirements, and suitability for miniaturization, making them ideal for point-of-care applications in virus detection. This review comprehensively summarizes the recent progress of photonic biosensor technologies, focusing on wavelength shift and luminescence-based mechanisms. We look into their operational principles, general configurations, and the challenges associated with these technologies. We further present an overview of the material developments used in photonic biosensors, encompassing organic, inorganic, and hybrid composite-based materials. The discussion extends to surface functionalization using biorecognition elements, including DNA/RNA, aptamers, and antibodies, to craft the specificity of the photonic biosensors for viruses. Ultimately, we emphasize the importance of a multidisciplinary approach in developing new materials architecture, biological receptors, and modifications to photonic methods, aiming to realize better biosensors for virus detection with ultra-high sensitivity, rapid response, and excellent selectivity.

1. Introduction

The outbreak of novel coronavirus disease 2019 (COVID-19) first identified in early December 2019, has rapidly evolved into a global pandemic. As of August 30, 2023, the World Health Organization (WHO) reported 770 million confirmed cases of COVID-19 worldwide, with 6.9 million fatalities. COVID-19 outbreaks are caused by the severe acute respiratory syndrome coronavirus 2 (SARS-CoV-2), classified as an enveloped virus,[1] which has high infectious rates and has mutated into several variants (such as Alpha, Beta, Gamma, and Omicron).[2] Previous outbreaks, including influenza, Zika, Ebola, SARS-CoV, and Middle East respiratory syndrome (MERS), were also caused by enveloped viruses that uses glycoproteins to bind with the host cells.[1] Additionally, non-enveloped viruses (e.g. enteroviruses,[3] adenoviruses) also pose a threat to human health by binding with the host cells through glycoprotein spikes that

sprout from the capsid.[1] The swift spread of the virus, coupled with initial unpreparedness in detection methodologies, has led to significant challenges in public health management. Several detection methods have been introduced to mitigate the transmission of viruses. Imaging techniques, such as chest computed tomography (CT) scans[4] and chest radiographs[5], have emerged as practical diagnosis tools with high accuracy in the hospital. However, these methods require a high cost and a specialist physician to interpret results.[4] Alternatively, serology-based tests, including chemiluminescence immunoassay (CLIA),[6] lateral flow immunoassay (LFIA),[6] enzyme-linked immunoassay (ELISA)[7], offer more accessible diagnostic options. Unfortunately, while affordable, ELISA falls short in providing quantitative analysis, exhibits low sensitivity (87.3%), and requires long sample-to-results time (over 4 hours).[7, 8] Although rapid antigen tests facilitate prompt detection, their effectiveness is compromised by low sensitivity and influenced by the specimen‘s quality, the viral load, and the patient’s condition.[9] Currently, reverse transcription-PCR (RT-PCR) is considered the gold standard for monitoring virus infection.[10] RT-PCR stands out for its specificity and sensitivity in viral RNA detection, yet it demands skilled operators, high costs, and lengthy processing time.[11, 12]

The development of user-friendly, rapid, sensitive, and accurate biosensing methods for virus detection is critical for effectively controlling and preventing future outbreaks. Photonics and electrochemical biosensors stand out as the most prevalent methodologies in the biosensing field, particularly for their application in diagnostic technologies transitioning from laboratory settings to point-of-care diagnostics.[13] Photonics biosensors, distinguished by their compatibility with integration and miniaturization efforts, require minimal analyte volume, achieving sensitivity at the femtogram levels and facilitating single-molecule detection.[13] One of the most widely used photonics biosensors for real-time label-free detection is surface plasmon resonance (SPR) based biosensors.[14-17] However, the researchers have been modified and combined the SPR transduction mechanism to enhance its performance. For example, dual-channel prism-based SPR transducers have been developed to increase the sensing parameters of the sensors. This configuration enables the detection of HIV DNA hybridization and the DNA melting temperature changes in different channels at the same time.[18] Another research study also showed the use of fiber optics in SPR sensors to simplify the optical design and to be a candidate for portable point-of-care testing devices with rapid detection ability (around 20 minutes) of the SARS-CoV-2 virus.[19] The photonic biosensor to detect the SARS-CoV-2 virus has also been developed using silicon nitride rings as sensor chips and plastic micropillar fluidic cards. This disposable and cost-effective photonics sensor was used to detect antibodies of

SARS-CoV-2 antigens in human serum, addressing the challenge of the complexity of handling samples and the high cost of the sensor.[20]

The field of photonic biosensors for detecting diverse analytes has made significant progress over the last several decades. During the late 20th century, researchers primarily focused on using gold (Au) and silver (Ag) to induce surface plasmon resonance (SPR) phenomena for analyte identification.[21, 22] However, these methods had drawbacks, such as inadequate sensitivity, lengthy testing procedures, and limited selectivity. In response, early 21st century scientists developed more advanced methodologies to enhance the capabilities of photonic sensors. The advancements include the use of photonic crystals (PC), whispering gallery mode (WGM), and Förster resonance energy transfer (FRET). These techniques significantly improved the sensitivity, selectivity, and operational efficiency of the sensors. In the past decade, there has been a growing demand for better identification of organic substances and biomolecules. Inorganic-based sensor materials, however, have the potential to harm biomolecule samples, thus reducing the sensing performance.[23-26] Since 2016, research has increasingly prioritized the utilization of organic-based materials and composites to enhance the biocompatibility of the photonic sensors.[27-30] The urgency of such research was amplified by the COVID-19 pandemic in 2020. Consequently, a lot of efforts have been dedicated on integrating biological receptors into photonic biosensors to detect various biomolecules and microorganism, including cancer cells, germs, and viruses.[30-33]

This review extensively covers the progress in photonics biosensors from 2018 to 2024, highlighting their potential in virus detection. We delve into various photonics structures, discussing their mechanisms based on wavelength shift and luminescence, and examine material design for photonics biosensors, including organic, inorganic, and hybrid materials. Furthermore, we summarize the option of bioreceptor units in photonic biosensors for virus detection, such as DNA/RNA, aptamers, and antibodies. In addition, we discuss the challenges of adopting a multidisciplinary approach in translating photonic biosensors for virus detection into practical applications, offering perspective on overcoming these challenges. This comprehensive review aims to serve as an invaluable resource for biosensing researchers in the field, contributing to the ongoing efforts to enhance diagnostic efficiency and quality through photonic biosensors.

2. Photonic (Bio) Sensing Mechanism

Photonic-based biosensors have been considered as an alternative route to obtain rapid and highly sensitive detector in various analytes.[13, 34] Despite its broad applications, the underlying science behind how the substance of interest is measured through optical signal is relatively simple. The analyte's concentration can be measured through two mechanisms, first is based on wavelength shift, and another is based on the luminescence. Wavelength shift in photonic-based biosensor can produce an ultrasensitive detector since wavelength is sensitive to the change of material's optical property.[35] When a specific analyte bound to the detector, it can induce a change in the photonic materials such as periodicity and the refractive index.[36, 37] This simple concept is employed and engineered further to expand and broaden the applications of photonic-based biosensor. Methods that use wavelength's shift as the measured signal including photonic crystals (PCs),[38] surface plasmon resonance (SPR),[39] and whispering gallery mode (WGM).[40] While luminescence-based biosensor detects the presence of analyte based on light generation mechanisms. Generally, they are two types of fluorescence-based biosensor which are Forster Resonance Energy Transfer (FRET)[41] and Luminescent Resonance Energy Transfer (LRET).[42] This section will discuss each mechanism and the corresponding methods. The general setup and how the signal is generated will be discussed for each method. Additionally, key factors that govern the sensitivity of each method described. Finally, advantages and challenges of each method are described within.

2.1 Photonic Crystal (PCs)

Photonic crystals (PCs) are a class of material having periodically arranged dielectric constant that can be tailored in 1D, 2D, and 3D direction.[38] Such arrangement uniquely features a photonic bandgap (PBG) in which electromagnetic waves with energy corresponding to this PBG are prohibited from propagating through the PCs hence reflected to the environment.[43] Any change in the dielectric constant or periodicity of the PCs resulting on different wavelength of the reflected light.

Typical set up of 1D PC, also known as Fiber Bragg Grating (FBG) is shown schematically in Figure 1A.[44] It consists of an optical fiber in which embedded with the FBG inside. When light with a specific input spectrum travels inside the optical fiber and strike the FBG, a certain wavelength called Bragg's wavelength (λ_B) whose value is governed by eq. 1, will be reflected back, thus the transmitted spectrum will have a peak in the wavelength value of λ_B as shown in Figure 1A. η_{eff} is the effective refractive index, and Λ is the FBG's periodicity. η_{eff} depends on

the fiber's and surrounding refractive index thus any change in the surrounding refractive index or the grating's periodicity will be detected as a wavelength shift in the value of λ_B as shown in Figure 1A.

$$\lambda_B = 2\,\eta_{eff}\,\Lambda \tag{1}$$

Different from 1D PC, 2D PC exhibits periodicity in two directions which make them show typical Debye diffraction ring.[37] This allows one to monitor the interparticle spacing (D) of 2D PC which related to the analyte's concentration by measuring the radius of the Debye diffraction ring (r).[45] In equation 2 and 3, λ is the incident wavelength, α is the forward diffraction angle, and h is the distance between sample and the screen.[46] Schematic and Real image of the Debye ring formation is shown in Figure 1B and 1C, respectively.

$$D = \frac{2\lambda}{3\,\sin\alpha} \tag{2}$$

$$\alpha = \tan^{-1}\left(\frac{r}{h}\right) \tag{3}$$

At present, PCs are quite challenging to fabricate due to the requirements of highly ordered structure. A small difference in periodicity or material's optical property can limit the performance of the PCs. Therefore, a simple approach can be developed through self-assembly, which does not need strict human control.[47] Many PCs are available in their solid state which requires the extraction of analytes to be measured. This can result in contamination, analyte loss, or other undesired chemical reactions.[48] Such disadvantages must be prevented to override unwanted drawbacks. Wearable or *in vivo* detection devices could solve this issues and being developed in the future for advance healthcare systems.[49] Although some PCs-incorporated hydrogel photonic biosensor have shown their great performance, water loses problem still remain challenging to be solved as it could degrade the sensor performance.[50] Therefore, an antifreezing ability of the hydrogel must be enhanced to overcome the current limitations.[51] Finally, materials selection and sensor configuration are very crucial since it will affect how will the bio-functionalization take place and the corresponding limit of detection.[52]

2.2 Surface Plasmon Resonance (SPR)-based Biosensor

Plasmon is a collection of electrons which oscillate under the influence of electric field from electromagnetic waves. Plasmon generation requires a material with free electrons and low optical losses such as gold (Au) and silver (Ag) nanoparticles.[53] When light hits the plasmonic

material, a specific wavelength that matches with the momentum of the conduction band of electrons is absorbed thereby generating surface plasma wave (SPW).[54]

Three ways in which light can generate SPW are through prism coupling, optical fiber waveguide, and diffraction grating as illustrated in Figure 1D. Using a prism, incident light will experience a total internal reflection (TIR) and the point where it is reflected generates evanescent wave (EW) which excite the SPW at the metal-dielectric interface. The same concept applies for the optical fiber waveguide where EW is the key to generate SPW. SPW propagates along the boundary between dielectric and a metal and is characterized by the propagation constant (β) and electromagnetic field distribution. The SPW field mostly lies on the dielectric region, which means a slight change in the dielectric refractive index resulting in different propagation behavior of SPW. Upon analyte binding, the refractive index of dielectric increases and so does the β value. The change of these parameters can be detected and interpreted as the analyte concentration which is the underlying principle of SPR-based biosensor. [55]

Although SPR based biosensor is widely investigated, still some challenges remain. SPR can only be generated through a specific materials with sophisticated and uniform structure, therefore material synthesis should be optimized to prevent non-uniformity in the biosensing device.[56, 57] Additionally, cluster of plasmonic nanoparticles are generally prepared through a top down process such as electron beam lithography and focused ion beam milling which suffer from low throughput and limited to in-plane fabrication.[58] Similarly, bottom up approaches through a self-assembly process limited to the ease of functionalization into the nanogaps.[59] From biocompatibility aspect, having metals contact with human's body is not desired since it potentially generates an inflammatory response which aggravate patient's condition. Therefore, plasmonic materials with enhanced biocompatibility is needed to enable *in vivo* biosensing.[48] Since LOD and the assay time are inversely corelated, enhancing one factor results in decreasing of the other one. SPR based photonic biosensor has its advantages on enhancing fluorescence signal which then can be coupled to obtain dual-enhanced plasmonic biosensing for accurate and rapid detection.[60]

2.3 Whispering Gallery Modes (WGMs)

Whispering gallery modes (WGMs) is an approach to detect even a trace quantity molecule.[61] The principle is based on light confinement in a small (typically micro sized) cavities such as

microsphere,[62] microring,[63] microcylinder,[64] and microtoroid.[65] When a light with specific wavelength is coupled with microcavities with one of the specific resonances, it will travel in a circular path due to the total internal reflection, hence the low threshold light power is amplified and produce a high intensity light according to equation 4

$$I \approx \frac{Q}{V}\frac{c}{\omega}P_{input} \quad (4)$$

I is the intensity of confined light, Q-factor depends on microcavities geometry, V is the volume of microcavities, c and ω depend on light properties, and P_{input} is the light's power. From equation 4, high I can be obtained by designing small sized microcavities with high Q factor. When analytes adhere to the microcavities, the resonating wavelength will experience a shift that can be approximated according to equation 5.[61]

$$\Delta\lambda \approx \frac{t}{R}\lambda \quad (5)$$

Δλ is the wavelength's shift, t is the analyte's layer thickness, R is the microcavities radius, and λ is the original resonating wavelength.

Preparing high Q-factor microresonator is the main challenge in WGM based biosensor.[66] Moreover, WGM based biosensor still lack chemical stability of some of the cavity materials in water and still need to be optimized further to not perturbing biological cell or organism.[67] Interestingly, recent research reported about deformed microcavities which can achieved Q factor up to 10 million. The remarkable finding was attributed to the fast momentum transformation in optical microresonators.[68] Finally, optimization of ultra-sensitivity together with large detection area is highly desired since these two factors are often related inversely.[69] Future works can be directed to work on solving these issues which might open WGM-based biosensor for more diverse applications.

2.4 Forster Resonance Energy Transfer (FRET)

FRET is a non-radiative energy transfer that occurs by dipole-dipole coupling from an excited state donor (D) to a ground state acceptor (A) when appropriate spectral overlap and proximity requirements are satisfied.[70] Appropriate spectral overlap can be achieved if the donor's emission and acceptor's absorption spectra are overlapping. FRET is famous for its ability to probe protein-protein interaction (typically within a distance 1-10 nm) since the energy transfer can only happen when A-D pair is close enough.[70] Basically, there are three key processes in

a FRET biosensor. First is the excitation of donor molecules due to light-matter interaction, second is the columbic interaction between D* and A and finally the induced dipole felt by A is manifested as the transition from A to A*. When A* returns to A, the energy will release in the form of light. If this emission is detected, then there must be an interaction between the associated proteins. However, if the emitted light is low in intensity thus no interaction between the proteins due to the presence of inhibitor which usually an analyte in this case. Illustration of the FRET process is shown in Figure 1E.

For example, Lao et al. use plasmon-enhanced FRET biosensor based on Tm^{3+}/Er^{3+} co-doped core-shell upconversion nanoparticles (scUCNP) to achieve ultrahigh sensitive virus detector.[71] When the virus concentration is low, PL signal shows a very strong peak indicating FRET is occurring since no inhibitor (virus) block the FRET process. However, when the virus concentration is increasing, the PL intensity got quenched which indicate viruses bind to the associate protein blocking the FRET process as shown in Figure 1F.

Despite its huge advantages on probing protein-protein interaction and commonly referred to "molecular ruler", FRET-based biosensor suffers from their low light emission which affect the detection limit.[72] in FRET based biosensor, the choice of donor and acceptor fluorescent proteins contribute significantly to the biosensor's sensitivity which must be carefully selected. Similar to any photonic system, long lifetime of donor excited state is often desired. However, common fluorophore used typically has low lifetime which start the development of lanthanide-based FRET (LRET).[73]

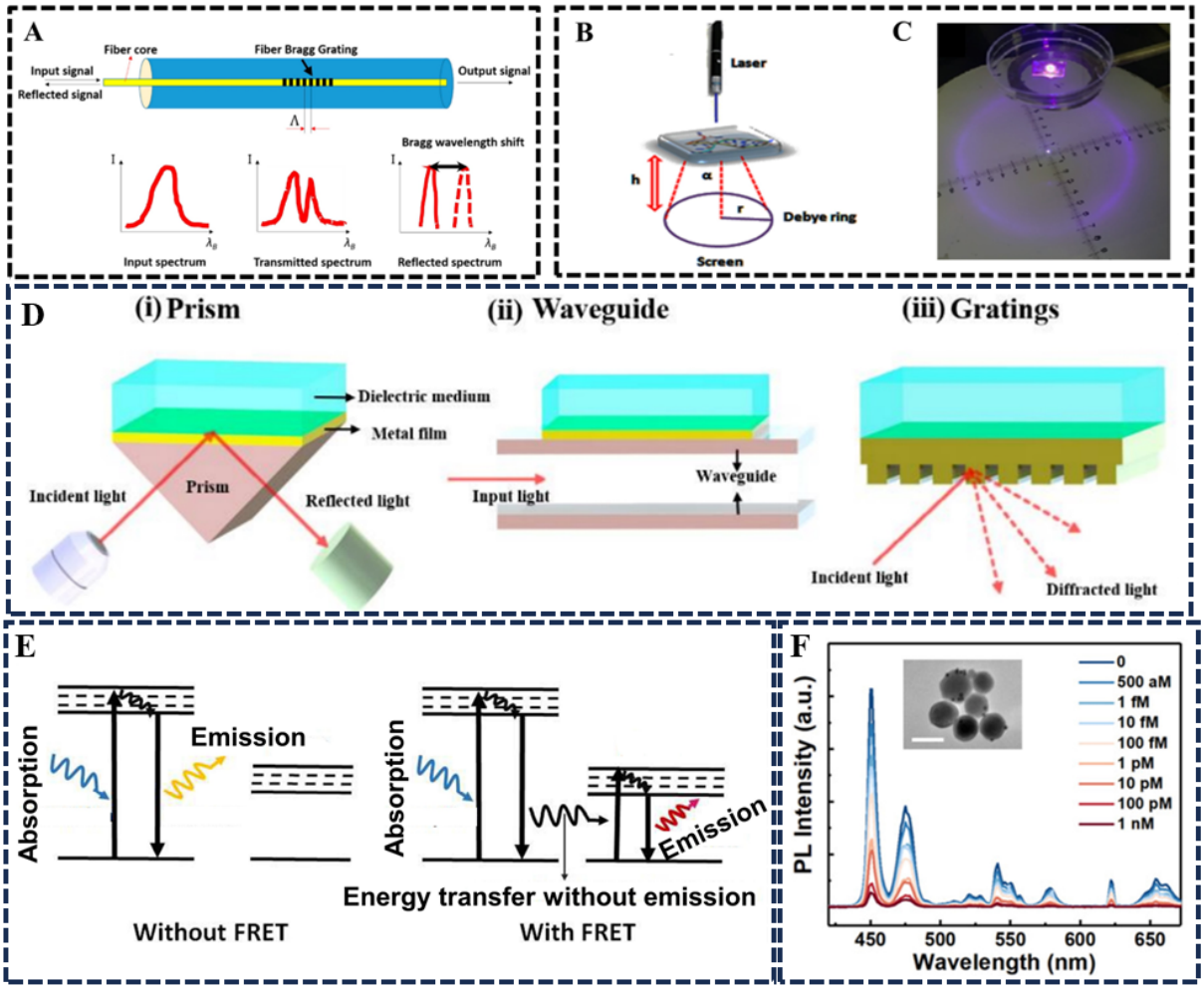

Figure 1. A) Typical setup for FBG photonic biosensor. B) Schematic illustration of Debye ring formation C) Actual experiment. D) Mechanism to generate surface plasma wave. E) Illustration of light matter interaction without FRET (left) and with FRET (right). F) PL spectra of csUNCP decreasing as the concentration of SARS-CoV-2 increasing. A) Reproduced with permission and modified from ref.[44] Copyright 2018, MDPI. B, C) Reproduced with permission from ref.[74] Copyright 2023, Elsevier. D) Reproduced with permission from ref.[75] Copyright 2022, MDPI. E) Reproduced with permission from ref.[76] Copyright 2018, Royal Society of Chemistry. F) Reproduced with permission from ref.[71] Copyright 2023, Wiley Online Library.

3. Materials Design for Photonic Biosensors

The quality of photonic biosensing performance is intrinsically linked to the selection of active materials within the system. This section provides an overview of materials commonly integrated into photonic biosensor, categorizing into inorganics, organics, and composite materials, and discusses their general properties alongside innovations in material design. The

comparison of inorganic, organic, and hybrid materials in biosensor applications is shown in Table 1.

3. 1 Inorganic Materials Based for Photonic Biosensors

Inorganic materials, such as Ag, Au, and Ti, are commonly used materials for photonic biosensors, which are favored due to their high mechanical strength for deformation resistance, remarkable stability against environmental changes, good reproducibility, and tunable optical properties.[77, 78] This section highlights recent advancements in employing these materials in photonic biosensors.

A modeling study was conducted on a highly sensitive photonic crystal fiber (PCF)-based surface plasmon resonance (SPR) sensor layout utilizing a dual-layer PCF with an outer layer made of gold (Au) with a thickness of 35 nm, exhibiting a negative real permittivity. A perfectly matched layer (PML) within a circular array is applied to enhance sensor performance. The resulting design features symmetrical air hole structures, including three small air holes in the second layer and a central hole to improve the evanescent field. The proposed layered model appears in Figure 2A where optimal parameter variations are obtained when the air hole diameter rc = r2 is 0.2 μm, r1 is 0.4 μm, the thickness of the gold (Au) layer is 35 nm, and the pitch/spacing between the air holes is 2 μm. Waveguide length and amplitude interrogation methods are used, showing a maximum sensitivity of 9000 nm/RIU and amplitude sensitivity of 318 RIU^{-1} (Figure 2B) with a maximum resolution of 1.11×10^{-5} within a detection range between 1.34 and 1.37. The results indicate that this model can be effectively used in biochemical and biological analytics detection, with significant potential applications.[79]

Further, research into a photonic device based on Stibnite-Titanium Nitride-Hyperbolic Metamaterial (Sb_2S_3-TiN-Hyperbolic Metamaterial) has been successfully developed operating in the visible frequency spectrum. Hyperbolic Metamaterial exhibits low losses and is activated through a prism-coupling scheme, allowing guided modes to be excited at visible frequencies. An adjustable plasmonic biosensor has also been designed to detect biotin at a concentration of 1 pM/L and thrombin as small as 1 fM/L. This sensor demonstrates adjustable differential response, enabling the detection of biomolecules with both high and low molecular weights. The adjustment of the Goos-Hänchen shift of the sensor is enhanced through the use of a high-index prism and appropriate excitation wavelength. Test results indicate maximum adjustment at the visible wavelength, improving wavelength stability and measurement precision.[80]

In addition, a dual-functional plasmonic biosensor using two-dimensional gold nano islands (AuNIs) has been developed to detect the SARS-CoV-2 virus. This sensor combines the photothermal plasmonic effect with localized surface plasmon resonance (LSPR) sensor transduction, providing an alternative solution for the clinical diagnosis of COVID-19. The AuNI sensor chip is fabricated by producing an Au nanofilm through a thermal de-wetting process. The thickness of the Au nanofilm is optimized around 5.0 to 5.2 nm and then annealed at 550°C for 3 hours. AuNIs are then assembled on a BK7 glass surface. With a low detection limit down to 0.22 pM, this sensor allows for precise detection of specific targets in multi-gene mixtures.[81]

Other research has successfully realized label-free photonic biosensors based on surface plasmon resonance but further interrogated the formation of Goos-Hänchen reflectance shift. The material used in this study is silver nanomaterial coated with a thin layer of $Ge_2Sb_2T_5$ (GST). The use of GST in this research is to protect the silver nanomaterial from degradation and to induce phase changes into singularities, thereby increasing sensor sensitivity. The results obtained in this experiment show sensitivity of 1.72×10^8 nm RIU^{-1} (refractive index unit), a detection limit of 6.97×10^{-7} RIU with a position resolution of 0.12 μm, and a figure of merit (FOM) of 4.54×10^{11} μm $(RIU \cdot °)^{-1}$. Additionally, in this study, the sensor has been tested capable of detecting cytokine biomarkers (TNF-α and IL-6) with a concentration of 1 μM and capable of detecting the presence of integrin on arginylglycylaspartic acid peptide samples with variations in Mn^{2+} concentration ranging from 1 nM to 1 mM.[82]

Several studies discussed, provide insights into the development of inorganic materials for use as photonic biosensors capable of utilizing various common principles of photonic biosensors such as surface plasmon resonance, photonic crystal, and surface-enhanced Raman scattering, as well as combinations of these methods. The development results in the ability of materials to detect various analytes and improve detection limits. However, despite modeling results, experimental outcomes still show limitations in detection using certain materials, relatively low biocompatibility, expensive materials cost, oxidization phenomena, and high detection limits still pose challenges in the development of inorganic materials as optical biosensors.[78, 83, 84] Therefore, alternative materials or designs are needed to address these issues.

Other materials such as graphene-based materials can address issues related to the low sensitivity. Graphene is a 2D nanomaterial with a thickness of only one atom, possessing excellent electrical conductivity, mechanical, optical, and chemical properties.[85, 86]

Additionally, it enhances material stability against surface oxidation phenomena commonly encountered in silver materials.[85] These properties make graphene a promising candidate as a primary or supporting material in photonic biosensor applications. The detection capability of photonic biosensors can be optimized through several advanced studies, both in numerical modeling and experimental approaches, that integrate metal materials with graphene.

A numerical modeling was successfully conducted to develop a photonic biosensor utilizing the surface plasmon resonance method, employing silver nanoparticles, TiO_2, and graphene as the main sensor materials. Silver is chosen for its excellent plasmonic properties, while graphene is selected for its high conductivity, especially in the infrared spectrum, thereby enhancing detection sensitivity. Moreover, graphene exhibits excellent molecular absorption capabilities, further enhancing the sensor response to analytes. The use of TiO_2 is aimed at protecting silver from oxidation and improving its interaction with analytes. The modeling was performed using the finite element method and operated in the wavelength range of 1.5-1.9 μm. The results demonstrate sensitivity variations in the range of 500–4250 nm/RIU with a wide operating bandwidth, indicating the potential of this structure to detect diverse analytes.[87]

Other modeling-based research has successfully developed a photonic biosensor utilizing nano composite SPR methods. The materials used include: Aluminum (Al), Gold (Au), Silicon dioxide (SiO2), Graphene (G), and Gadolinium-Zinc Oxide (GZO). By modifying the thickness of each laminate, the radius of Al and G, as well as the chemical potential values of each material, testing capabilities were achieved within the wavelength range of 300-600 nm, with a detection sensitivity of ~664.8 nm/RIU, and the ability to detect various strains of the coronavirus. The results of the coronavirus strain variations testing are presented in the UV-Vis results, where the samples are able to exhibit distinct spectrum peaks for samples of Avian Fowl Adenovirus (FAdV), Infectious Bronchitis Virus (IBV), Highly Pathogenic Avian Influenza Virus (H5N1 and H5N2), Avian Influenza Virus (H9N2), and Influenza Virus (H4N6).[88]

3.2 Organic Materials Based for Photonic Biosensors

Some properties of the synthetic organic-based polymer and biopolymer materials in general, include relatively better biocompatibility than inorganic materials, higher detection limits, and the ability to provide a conducive environment for biomolecules, making it easier for biomolecules to be trapped in sensor materials, which in turn improves detection capabilities for biomolecules, and they are easier and cheaper to obtain.[89-92] Here are some biopolymers

and combinations of biopolymers with synthetic polymers used as photonic biosensor materials in the last several years.

Alginate is an anionic biopolymer that is primarily derived from brown algae. This material possesses water resistance, oil barrier characteristics, modified mechanical properties, superior antibacterial capabilities, sensitivity to ammonia, and color stability.[93] These properties, supported by biocompatibility, biodegradability, and the ability to modify its photonic structure, have the potential to make it suitable for applications as a sensor in liquid substances.

A successful study was conducted to create a highly sensitive flexible photonic pressure sensor, integrated with various environmental stimuli that has been used in multiple applications. This sensor is built on a three-dimensional photonic crystal lens combined with alginate-based hydrogel. Low-pressure stimuli can cause small changes in the photonic bandgap, resulting in a shift in the maximum frequency and variation in the amplitude of reflected light. Thanks to the significantly amplified reflection spectrum and structural color shift, this sensor with a diameter of 310 nm demonstrates ultra-high sensitivity of 32,3 kPa^{-1}, a peak shift of 30 nm, and a fast response time of about 0.21 s. When comparing sensitivity values with other studies, such as pressure sensors based on acrylamide-based hydrogel and polyvinyl alcohol (PVA) with a sensitivity of 0.05 kPa^{-1},[94] and pressure sensors made from amorphous calcium carbonate nanoparticles combined with polyacrylic acid and ALG with a sensitivity of 0.17 kPa^{-1},[95] the sensitivity value obtained here is significantly higher. Furthermore, when compared to the detection limit values of other studies, including organic polymer diode pressure sensors (OLEDs) with a detection limit of 1.4 kPa,[96] the detection limit obtained in this study is much better. Furthermore, the density, sound speed, and acoustic impedance of this photonic sensor are in accordance with water. Therefore, this sensor provides a promising strategy for future-generation flexible photonic acoustic sensor devices.[97]

Cellulose is a polymer consisting of long chains of β-D-glucose units linked via β-(1-4) bonds. This structure gives it unique properties related to photonic structures, especially when transformed into nanoscale cellulose crystals (CNCs) for use in photonic applications. The repeating and regular structure, where each glucose unit is bound to the next through β-(1-4) bonds, enables the formation of nanoscale cellulose crystals with a periodic structure.[98] This periodicity can create interference phenomena and light reflection, impacting iridescence properties.[99] Moreover, the ordered orientation of cellulose chains imparts birefringence properties, meaning that light passing through cellulose may have two different refractive

indices depending on the light's polarization.[100] This creates optical effects that can be harnessed in photonic structures. The helical structure present in CNCs also provides characteristic chiral properties that can influence optical characteristics and allow the formation of cholesteric liquid crystal (LC) phases with chiral optics.[98] Additionally, the helical pitch length of CNCs can be controlled, allowing for the adjustment of reflected wavelength, thereby influencing the color and other optical properties emitted by the photonic structure of CNCs.[91]

An experiment about an organic gel derived from cellulose has been successfully developed, demonstrating dynamic properties and well-controllable structural colors. The gel is created using a hydroxypropyl cellulose (HPC) matrix at 68 wt%, with the addition of different polyethylene glycol (PEG) guest molecules. The role of PEG is to regulate the reflective color of HPC gel by accurately placing them on the backbone of HPC helices through electrostatic repulsion. Furthermore, the gel exhibits remarkable dynamic properties in response to temperature, pressure, and strain. The rapid, continuous, and reversible color changes make this gel highly promising for applications in various fields.[101] This research opens the door to the development of optical sensors with high stability and flexibility, providing potential contributions to the advancement of sensor technology, especially in virus detection systems.

Chitin is a polysaccharide that can be found in the exoskeleton of arthropods, particularly in the subphylum crustacea, where 20–30% of the crustacean's composition is chitin.[102] Its structure is analogous to the chemical structure of cellulose, but the hydroxyl groups at the C2 position are replaced by acetamido groups.[103] This structural difference, when compared to other polysaccharides, gives chitin an additional ~6 percent of nitrogen.[104] The presence of both major groups can interact to form hydrogen bonds, potentially causing chitosan molecules to form helices, similar to the helicoidal structure in chiral nematic liquid crystal optics. This property can create the effect of circularly polarized light reflection, resulting in bright iridescent colors displayed by some animals such as beetles, butterflies, and mantis shrimp.[89] However, the acetamido groups in chitin can form very strong interlayer hydrogen bonds, giving chitin the ability to be insoluble in most solvents.[104] Therefore, a method is needed to address this issue.

Partial deacetylation through alkali hydrolysis of chitin can transform it into chitosan, resulting in a linear polysaccharide containing N-acetyl-D-glucosamine and D-glucosamine units linked by β-(1-4) glycosidic bonds.[104, 105] The presence of primary amine groups ($-NH_2$) in each D-glucosamine imparts higher solubility to chitosan at pH levels, making it a potential material

for pH-responsive photonic crystal structures.[90] The chemical structure and specific molecular arrangement of chitosan also impact its selective light absorption and reflection abilities, such as low absorption in the UVC region.[106] In addition, it also possesses excellent biocompatibility, biodegradability, and is cost-effective.[89, 106, 107] The properties possessed by chitosan make it potentially modifiable as a biopolymer material with a photonic crystal structure.

Research demonstrates that inverse opal photonic crystal films (IOFs) made using chitosan, a biomacromolecule found in nature, can rapidly respond to alcohol and phenol, exhibiting reversible changes in structural color and reflection peaks. IOFs with specific pore sizes (201–319 nm) show good reproducibility and stability in organic solvents, making them potentially applicable in various fields. Chitosan in IOFs provides excellent electrochemical reactivity and biocompatibility, which can be employed for detecting chemical compounds or evaluating the quantity of organic compounds in aqueous solutions. In conclusion, these chitosan IOFs have the potential for use as visual detectors in environmental management and chemical analysis.[108]

Moreover, another study was conducted with the aim of creating three-dimensional gyroid-shaped photonic crystals using polystyrene-polydimethylsiloxane block copolymers to simplify and make the structure fabrication mechanism more cost-effective. To address the low absorption capability, chitosan was incorporated. In this context, the block copolymer serves as a template, while chitosan plays a role as the gyroid-shaped photonic crystal structure. With its low absorption capacity and high reflectance, chitosan has the potential to be applied in UV-based electronic devices.[106]

Another study successfully developed a fluorescence-based detection system, as demonstrated in this research. This research successfully developed a tobacco mosaic virus (TMV) detection system using a fluorescent biosensor with the Activators Regenerated by Electron Transfer Atom Transfer Radical Polymerization (ARGET ATRP) method, chitosan was employed as a material serving as a specific aptamer to recognize and capture TMV's RNA target, as can be shown in Figure 2C. Subsequently, chitosan would bind to propionic acid through a click chemistry reaction, forming multiple active sites for fluorescent polymerization. This process leads to an increase in fluorescence intensity, providing a second signal amplification effect. This capability lowers the detection limit to 1.14 fM, thereby enhancing the sensor's sensitivity.

Figure 2D displays the research results about fluorescence intensity based on the materials, while Figure 2E displays the research results about the sensitivity of the sensors.[109]

Several research findings have demonstrated high biocompatibility, good detection limits, and excellent selectivity and sensitivity in detecting biomolecules. However, some issues such as poor mechanical and chemical stability, which are related to the degradation capability of the biosensor, as well as the complex synthesis process, remain problematic.[77] Therefore, new innovations are needed to address these issues without reintroducing the problems associated with inorganic materials.

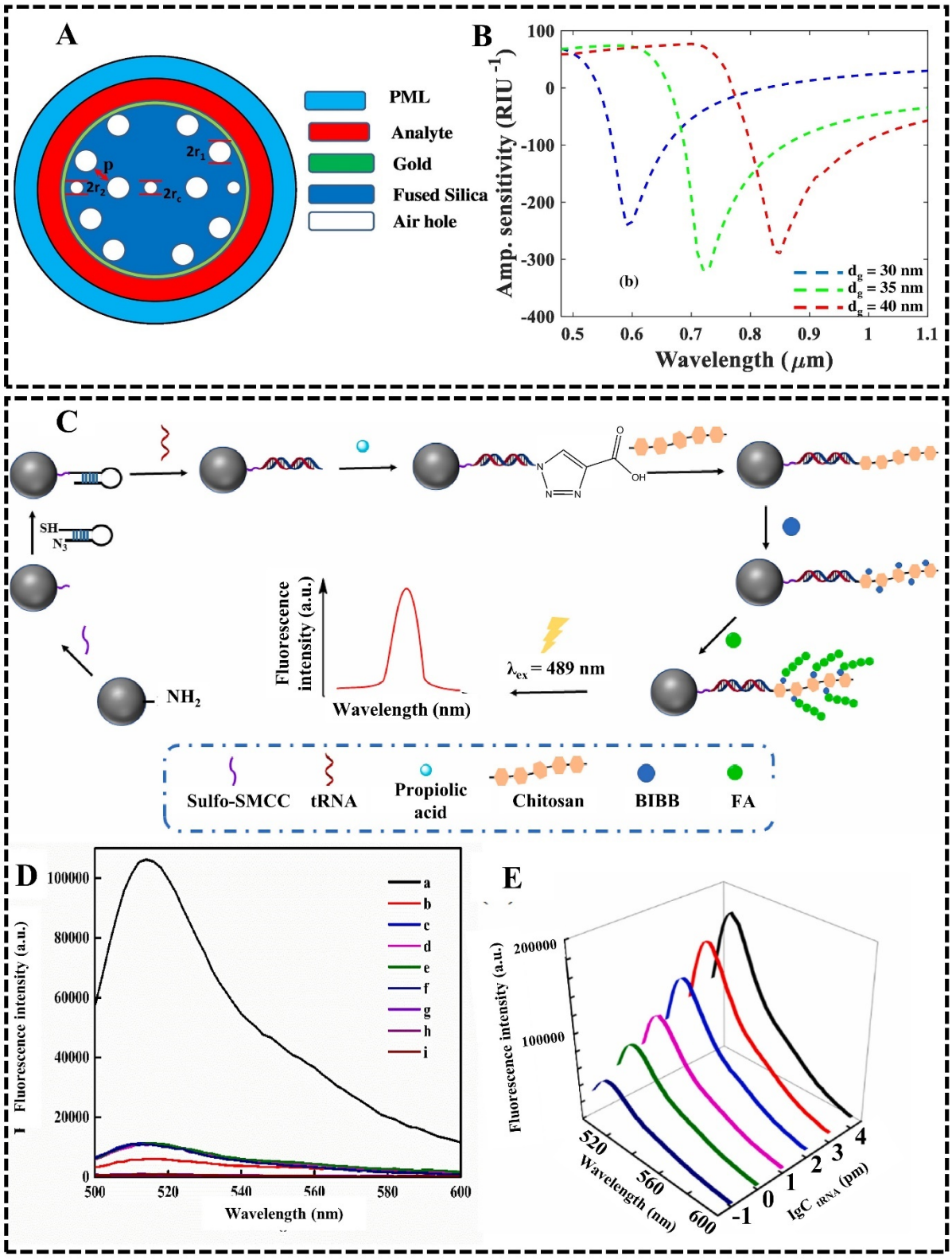

Figure 2. A) Designing views of the proposed circular lattice PCF sensor. B) Amplitude sensitivity for different thickness of gold layer. C) Fluorescence modification process based on ARGET ATRP/ chitosan signal amplification and detection principle. D) Fluorescence intensity curve of (a) MBs/Sulfo-SMCC/hDNA/RNA/PA/Chitosan/BIBB/FA, (b) in the absence of

hDNA, (c) RNA, (d) PA, (e) Chitosan, (f) BIBB, (g) FA, (h) solvent for testing, and (i) PBST buffer. E) Fluorescence intensity curve with different concentration of TMV RNA. A,B) Reproduced with permission from ref.[79] Copyright 2018, Elsevier. C, D, E) Reproduced with permission and modified from ref.[109] Copyright 2023, Elsevier.

3.3 Hybrid Inorganic Organic Materials Based for Photonic Biosensors

In general, the weaknesses of inorganic materials can be overcome by organic materials, and vice versa. This underpins the development of hybrid biophotonic materials. All these individual shortcomings can be addressed by adding inorganic particles into organic materials to form hybrids, where the inorganic material is used as a protective layer for the organic material, or vice versa, or both materials can provide positive synergistic effects.[77] Therefore, we will discuss several studies that have successfully developed hybrid sensors.

There has been development in utilizing chitosan as a virus detection material employing the colorimetric detection principle, which involves the modification of photonic structure. A successful experiment was conducted to create a TiO_2/Chitosan-nanocapsule-retinoid acid visualization sensor developed through alternate spin-coating for leukemia detection, as can be shown in Figure 3C. Researchers utilized chitosan material with a photonic crystal structure as the leukemia detection material. The researchers achieved the synthesis of a visual sensor, where a color change occurs due to the presence of specific proteins in the blood sample through its photonic bandgap structure, as can be shown in Figure 3A and 3B. This provides rapid and accurate diagnostic information about the presence of leukemia.[110] Thus, this research demonstrates the potential use of chitosan as a material for virus biosensors.

Research has successfully developed an innovative method for the fabrication of composite photonic crystal microspheres by integrating polymerization and self-assembly processes. Typically, traditional photonic crystal microspheres have internal pores and are created through the self-assembly of colloidal nanoparticles, leading to vulnerability to contamination and less satisfactory structural stability. In this study, composite organic-inorganic photonic crystal microspheres of SiO_2-Poly(2-hydroxyethyl methacrylate) (PHEMA) were created using the Shirasu porous glass (SPG) emulsification membrane. This process involved colloidal nanoparticles, monomers, and initiators in the continuous phase, undergoing polymerization and self-assembly to form composite microspheres. The primary advantage of this approach lies in the high structural stability achieved as colloidal nanoparticles are trapped within a crosslinked polymer network. The resulting composite microspheres not only exhibit superior

structural stability compared to traditional photonic crystal microspheres but also possess high color saturation and good hydrophobic properties. These advantages stem from the enhanced self-assembly of materials during polymerization, driven by hydrogen bond formation. Additionally, these SiO_2-PHEMA composite microspheres have various potential applications, including use as dyes, biosensors, and in illumination. Furthermore, the quick and straightforward production process makes this synthesis method potentially suitable for mass production and practical applications.[111]

Another study demonstrates successful synthesis of a photonic biosensor made of polystyrene (PS) combined with gold nanoparticles (AuNPs), as can be shown in Figure 3D. The first experiment aimed to compare the electrochemiluminescence (ECL) emission between non-structured PS and photonic crystal-structured PS using a dip and coating method, as can be shown in Figure 3E. The intensity results indicated that the photonic crystal-structured PS exhibited higher emission values (0.22) compared to the non-structured PS (0.10). Subsequently, surface enhancement (SE) treatments were applied to both PS samples by adding gold nanoparticles. The results showed that the ECL emission enhancement in non-structured PS was significantly smaller (0.13) compared to the photonic crystal-structured PS (0.92). Further analysis using electromagnetic wave simulations revealed that the ECL enhancement was caused by the electromagnetic field coupling on the surface of PS PhCs and Au NPs. Therefore, SE-ECL in materials with photonic crystal structures exhibited a detection range from 1 pg/mL to 1 μg/mL with a detection limit of 0.41 pg/mL (S/N = 3). This indicates the potential use of these hybrid materials for biomolecular applications.[84]

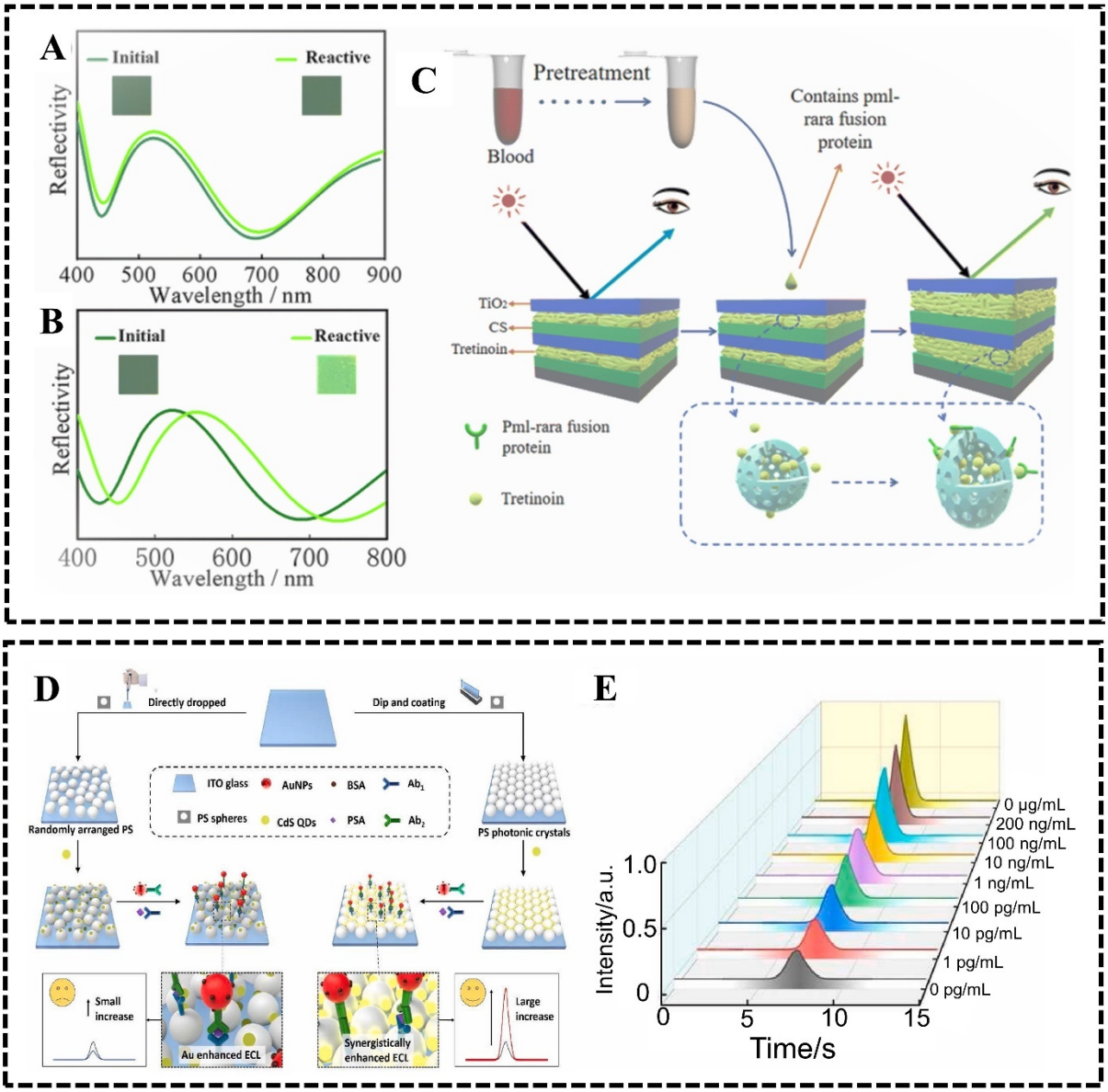

Figure 3. A) Visual sensor detects color changes in normal human blood samples before and after. B) Visual sensor detects color changes in acute promyelocytic leukemia (APL) blood samples before and after. C) Visual sensor detection mechanism. D) A schematic illustration of the difference between randomly distributed and non-randomly distributed photonic structures, which are then synergistically enhanced by ECL biosensors. E) Quantifying the sensitivity of the biosensor (PS-ECL) throughout a spectrum of concentration variations. A, B, C) Reproduced with permission from ref.[110] Copyright 2023, RSC Advances. D, E) Reproduced with permission from ref.[84] Copyright 2024, Elsevier.

Table 1 Comparison of organic, inorganic, and hybrid materials for biosensor applications

Materials Type	Materials	Method	Target analyte	Sensitivity	Selectivity	Rapid Detection	Ref

Inorganic	Au	PCF-SPR based	Biochemical and biological analytes (simulation)	9000 nm/RIU	Yes	n.a	[79]
	Sb_2S_3-TiN-Hyperbolic Metamaterial	SPR	Biotin	1 pM/L	Yes	30 min	[80]
			Thrombin	1 fM/L	Yes	30 min	[80]
	AuNIs	LSPR with thermo plasmonic sensor	SARS-CoV-2	0.22 pM/L	Yes	~17 min	[81]
	AgNPS coated with $Ge_2Sb_2T_5$	SPR with Goos-Hänchen reflectance shift	Cytokine biomarkers (TNF-α and IL-6)	1 μM/L	Yes	n.a	[82]
			Integrin on arginylglycylaspartic acid peptide	1 nM/L	Yes	n.a	[82]
	AgNPs-TiO_2-Graphene	SPR	Biochemical and biological analytes (simulation)	500-4250 nm/RIU	Yes	n.a	[87]
	Al-Au-SiO_2-Gadolinium-Zinc Oxide (GZO)	SPR	Avian Fowl Adenovirus (FAdV), Infectious Bronchitis Virus (IBV), Highly Pathogenic Avian Influenza Virus (H5N1 and H5N2), Avian Influenza Virus (H9N2), and Influenza Virus (H4N6	300-600 nm/RIU	Yes	n.a	[88]
Organic	Chitosan	Photonic crystal	Tobacco Mosaic Virus (TMV)	1.14 fM/L	Yes	n.a	[108]
	Alginate	Photonic crystal	Biochemical (simulation)	32.3 kPa^{-1}	Yes	0.21 s	[97]

		combine with pressure sensor					
	Hydroxypropyl cellulose	Photonic crystal	Virus (simulation)	n.a	Yes (with color change)	n.a	[101]
Hybrid Inorganic-Organic	TiO_2/Chitosan nanocapsule	Photonic crystal	Leukemia	n.a	Yes (with color change)	20 min	[110]
	AuNPS-Polysterene	ECL-Photonic crystal	Biomolecul (simulation)	0.41 pg/mL	Yes	n.a	[84]

555

556 **4. Surface Functionalisation of Photonic Biosensors for Virus Detection**

557 The recognition element is central to biosensors' functionality, directly interacting with target
558 analytes, and dictating the sensor's selectivity.[112, 113] The process of immobilizing these
559 recognition elements on the sensor's surface marks an essential stage in the development of
560 biosensors. Several functionalization methodologies, such as adsorption, entrapment, covalent
561 attachment, and electrostatic, can be employed.[114] This section mainly discusses on the
562 immobilization techniques and the effects of recognition elements, such as DNA/RNA, aptamer,
563 and antibodies, in the application for virus detection. The illustration of surface
564 functionalization for virus detection using the methods of Photonic Crystal (PC)[115], Surface
565 Plasmon Resonance (SPR)[116], Whispering Gallery Mode (WGM)[13], and FRET[117] can be
566 seen in Figure 4.

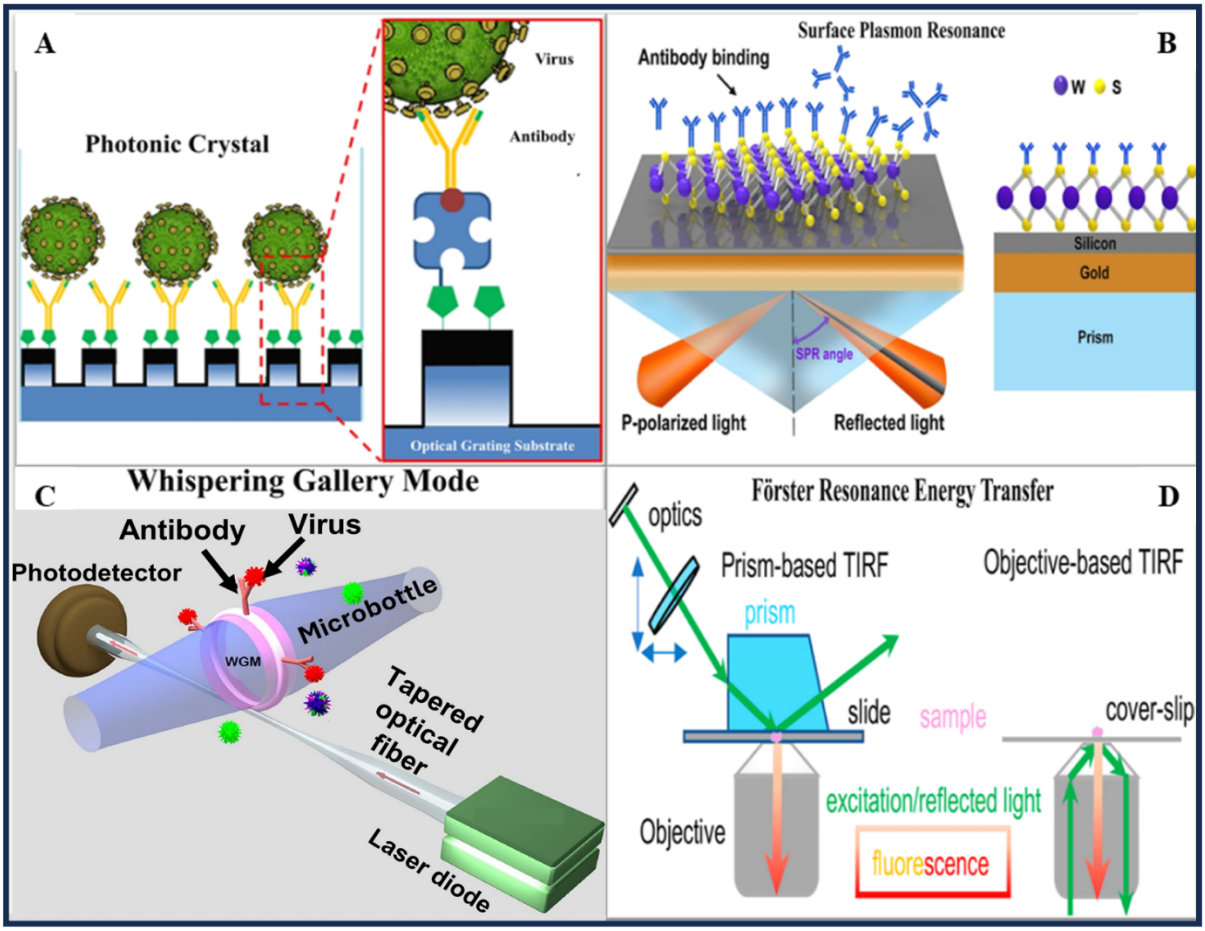

Figure 4. The illustration of detecting viruses and other biomolecules using the methods of A) Photonic Crystal (PC), B) Surface Plasmon Resonance (SPR), C) Whispering Gallery Mode (WGM), and D) FRET. A) Reproduced with permission from ref.[115] Copyrights 2014, Springer Nature. B) Reproduced with permission from ref.[116] Copyrights 2016, Springer Nature. C) Reproduced with permission from ref.[13] Copyrights 2022, De Gruyter. D) Reproduced with permission from ref.[117] Copyrights 2021, MDPI.

4.1 NA/DNA/RNA

Nucleic acid (NA) based diagnostics offer excellent sensitivity and accuracy for molecular detection since they directly target the hallmark regions of RNA viruses.[118] NA is a virus biomarker that contains the genetic information of bacteria or viruses.[119] The functional modification on the probe of the photonics sensor can serve the ultrasensitive and reduce the detection limit of NA.[119] The previous study used gold nanoparticles coated tilted fiber Bragg grating (TFBG)-based SPR to detect NA. The modification of gold nanoparticles with NA enhances the SPR response as illustrated in Figure 5A. The functionalization was done by Au-S bond using thiol end organic compounds at the 3 or 5 ends of the NA single strand. The self-assembled monolayer (SAMs) NA single strand-thiol probe on the gold nanoparticle surfaces

enables the NA single strands target to bind. The binding of NA target and gold nanoparticles attached NA probes resulting in the SPR enhancement due to local refractive index change on the gold nanoparticles surfaces.[119]

Several technologies have been developed to amplify the DNA to improve sensor sensitivity such as hybridization chain reaction (HCR), catalyzed hairpin assembly (CHA), entropy-driven reaction (EDR), and rolling circle amplification (RCA).[120] A novel approach in biorecognition elements has been developed in 3D DNA nanostructures to improve probe-analyte recognition. For example, tetrahedral DNA nanostructures-based DNA biosensors have been reported to improve hybridization efficiency, decrease background signal, and improve detection sensitivity significantly.[121] DNA origami is the self-assembly of long single-stranded DNA with the addressability of each nucleobase within its structures. These features allow the accurate positioning of target molecules or optically active particles.[122]

As for some examples of DNA Origami that we would like to show are nano DNA structures shaped like nets aimed to function as detectors capturing fluorescence signals when detecting and capturing SARS-CoV-2 virions. The structure created is a 4 x 4 DNA Net with a unit size of 42 base pairs where 5.89 nm represents the intratrimetric distance of the aptamer corresponding to the intratrimetric distance of SARS-CoV-2, and 14.96 nm is the size for maximum spike clustering. Research results indicate sensor capabilities equivalent to PCR (detection limit of 1000 copies of virus genome/mL), rapid testing (10 minutes) due to DNA Net's direct access to intact virus in the sample, eliminating the need for complex sample preparation, cost-effectiveness (~$1.26 per test, much cheaper than antigen ELISA at $5-$10 per test and lateral flow antigen-based tests at $20 per test), and operability at isothermal room temperature. Additionally, the developed sensor also has the potential to be a therapeutic sensor because of its ability to inhibit SARS-CoV-2 virus infection. Moreover, this sensor also has the potential to detect other viruses whose surfaces have class-I envelope glycoproteins, like other corona viruses and HIV.[123]

Furthermore, other research has successfully synthesized photonic sensors using the principle of detecting fluorescence intensity using DNA origami in 5 different structure variations, including DNA-bivalent, DNA-Linear, DNA-Star, DNA-Hexagon, and DNA-Heptagon, to detect the concentration of dengue virus (DENV2). The structures are expected to display aptamers targeting domain III of the dengue virus envelope protein (ED3) in a two-dimensional pattern corresponding to the spatial arrangement of ED3 clusters on the surface of DENV2. The

results show that the star-shaped DNA structure can produce the highest fluorescence emission in DENV2 testing at a concentration of 1 × 105 p.f.u./ml. Additionally, the star-shaped structure can also act as an inhibitor of DENV2.[124]

Other research has successfully used DNA origami beacons for biosensing applications. The working concept relies on properly positioned arrays of organic fluorophores. Two types of arrays, functioning as donor and acceptor fluorophores, form 48 fluorophore FRET pair, resulting in a large output signal for oligonucleotide detection applications (Cy3 and Cy5), as shown in Figure 5B. The positioning of donor and acceptor sites enhances detection sensitivity and selectivity. When the target DNA is missing, the DNA probe folds into a closed position (Figure 5C), bringing the donor and acceptor fluorophores close together. This facilitates FRET from the donor to the acceptor, resulting in decreased fluorophore emission (as seen in Figure 5D). Nevertheless, in the presence of the target DNA, the DNA probe unfolds (as shown in Figure 5E), resulting in a significant separation between the donor and acceptor molecules. This separation hinders FRET and leads to an enhanced emission of fluorophores, resulting in a color change to yellow and green, as shown in Figure 5E. The research findings show that the sensor's sensitivity allows it to detect concentrations as low as 100 pM/L with a detection time of 2 minutes, showcasing its strong selectivity capabilities.[125]

DNA walkers also show promise in biosensing applications since they can encourage cascade signal amplification for analyte detection that can be empowered by protein enzymes, DNAzymes, and strand displacement. To this extent, 3D DNA walkers have been frequently used to recognize proteins and nucleic acids.[126] The combination of DNA walker developed by the surface modification of aminated silica nanosphere and the fluorescence signal output can lower the false-positive signal risks.[126]

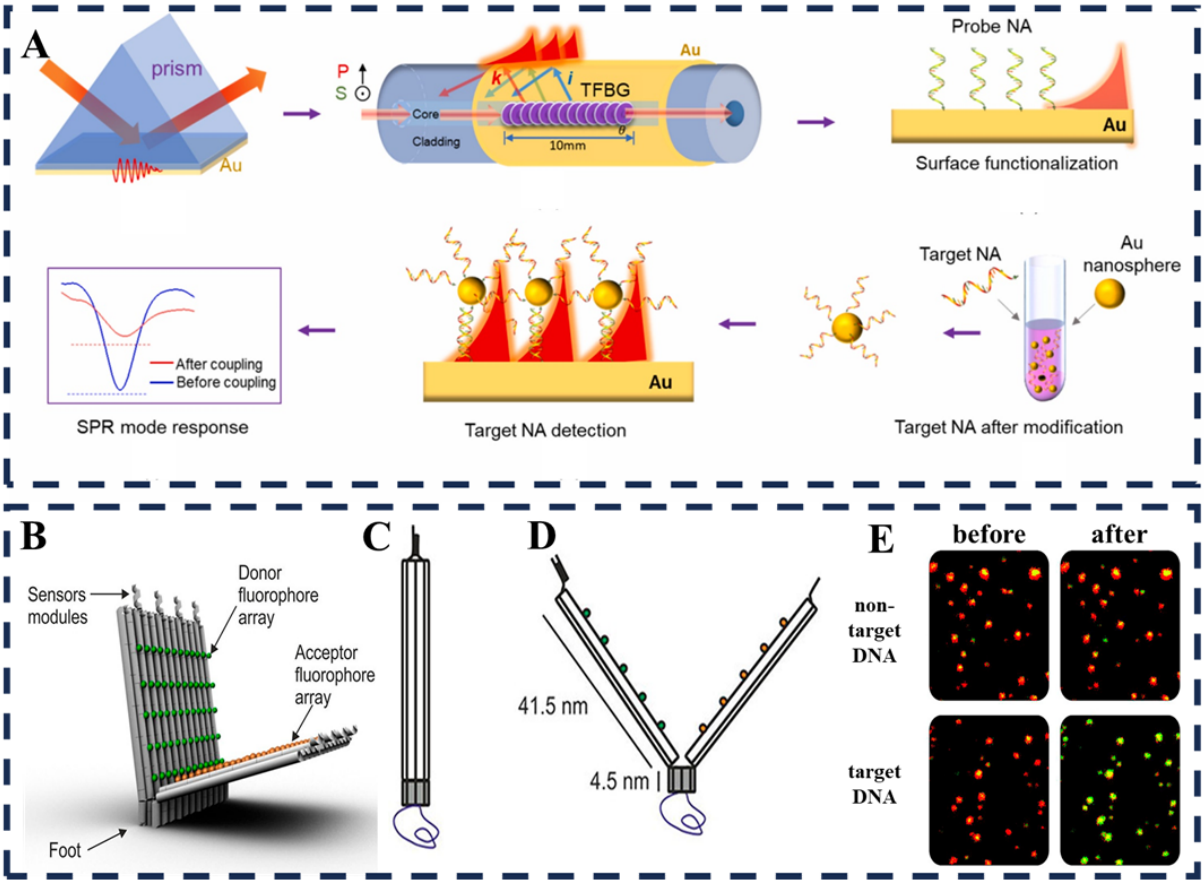

Figure 5. A) Schematic showing the design of nucleic acid modification on gold nanoparticle and its effect on SPR. B) Illustration of the DNA Origami Beacon (green dots represent donors and orange dots represent acceptors). C) Illustration of the closed mode when no target DNA is present and D) open mode when target DNA is present. E) Color change indicating an increase in fluorophore emission due to the presence of target DNA (Cy3 and Cy5). A) Reproduced with permission from ref. [119] Copyrights 2023, Elsevier. B, C, D, E) Reproduced with permission from ref.[125] Copyrights 2018, ACS Nano.

4.2 Aptamer

Aptamers are the special type of ssDNA or RNA oligonucleotides that are usually used as biorecognition elements in biosensors, known as aptasensors.[127] Aptamers are promising receptors that are potentially good for the integration with additional DNA-based signal amplification.[8] By using aptamers, high-specificity detection can be achieved with low cost, high affinity, and ease of modification.[6] In terms of COVID-19 detection, DNA aptamer serves high affinity to the S protein of the SARS-CoV-2 virus type including Alpha, Beta, Gamma, Epsilon, Gaba, Delta, and Omicron.[128] Previous studies modified the gold film surface by immobilizing it with DNA aptamers through the rapid freezing method. The Au-DNA was then incubated with 6-mercapto-1-hexanol (MCH) and bovine serum albumin (BSA) to hinder the

non-specific adsorption..[128] Using surface plasmon resonance imaging (SPRi) technique, the S protein will be captured by DNA aptamers inducing SPRi signal response. The addition of DNA aptamers-AuNPs on the SPRi systems improving its signal response, the limit of detection (LOD) of SPRi systems was 0.32 nM while after the DNA aptamers-AuNPs was 5.99 pM.[128]

The functionalization of gold-based sensor with ssDNA aptamer also previously reported for Dengue virus detection as can be seen in Figure 6A. The ssDNA aptamer against the non-structural NS1 protein functionalized the sensor to detect NS1 protein from blood. The blood plasma contains a high protein content that tends to concentrate on the gold surface, leading to protein fouling. One of the strategies to hinder the fouling was employ surface passivation using a thiol-terminated 6-mercaptohexanol self-assembled monolayer. The combination of surface functionalization using ssDNA aptamer and surface passivation was successful in detecting Dengue virus in bovine blood at a concentration of 0.1–10 μg/mL, with the addition of aptamer resulting the higher LSPR shift as shown in Figure 6B.[129]

Double-labeled DNA aptamers can be a recognition element for the sensitive detection of SARS-CoV-2 because the aptamer was shown to bind to the entire SARS-CoV-2 genome. Two modifications were done on the aptamer RBD-1C in the region of thiol-group to the 5′-end and Cyanine-3 to the 3′-end.[6] Altering the 5′ or 3′-end maintains the aptamer's affinity for the S-protein receptor-binding domain at nanomolar concentrations. The sensitivity of the sensor for SARS-CoV-2 detection is 100 copies/mL which is comparable with the PCR's limit of detection (10^2-10^3 copies/mL).[6]

The combination of ssDNA aptamer and photonic crystal was successfully built to detect HIV. The ssDNA aptamer was used to replace the RNA aptamer due to stability issues. ssDNA aptamer was crosslinked into a photonic crystal that has been self-assembly fabrication with polystyrene.[75] The interaction of gp120 (HIV) aptamer and protein was studied by molecular docking as can be seen in Figure 6C. The interaction starts from the carboxyl group of acrylamide monomer with EDC creating unstable o-acylisourea. The acrydite group contains -NH on the 5′ end of the aptamer produce a stable conjugate of aptamer with carboxyl group. The interaction of aptamer with virus was done through guanosine and thymine sequences that can visually change the material color from yellow-green to blue-green. The transmittance was detected using UV-Vis spectroscopy as can be seen in Figure 6D revealing the increasing of transmittance with the increasing of virus concentration. The LOD of this combination of aptamer-photonic sensor for HIV was 7.1 ± 1.55 ng mL^{-1}.[74]

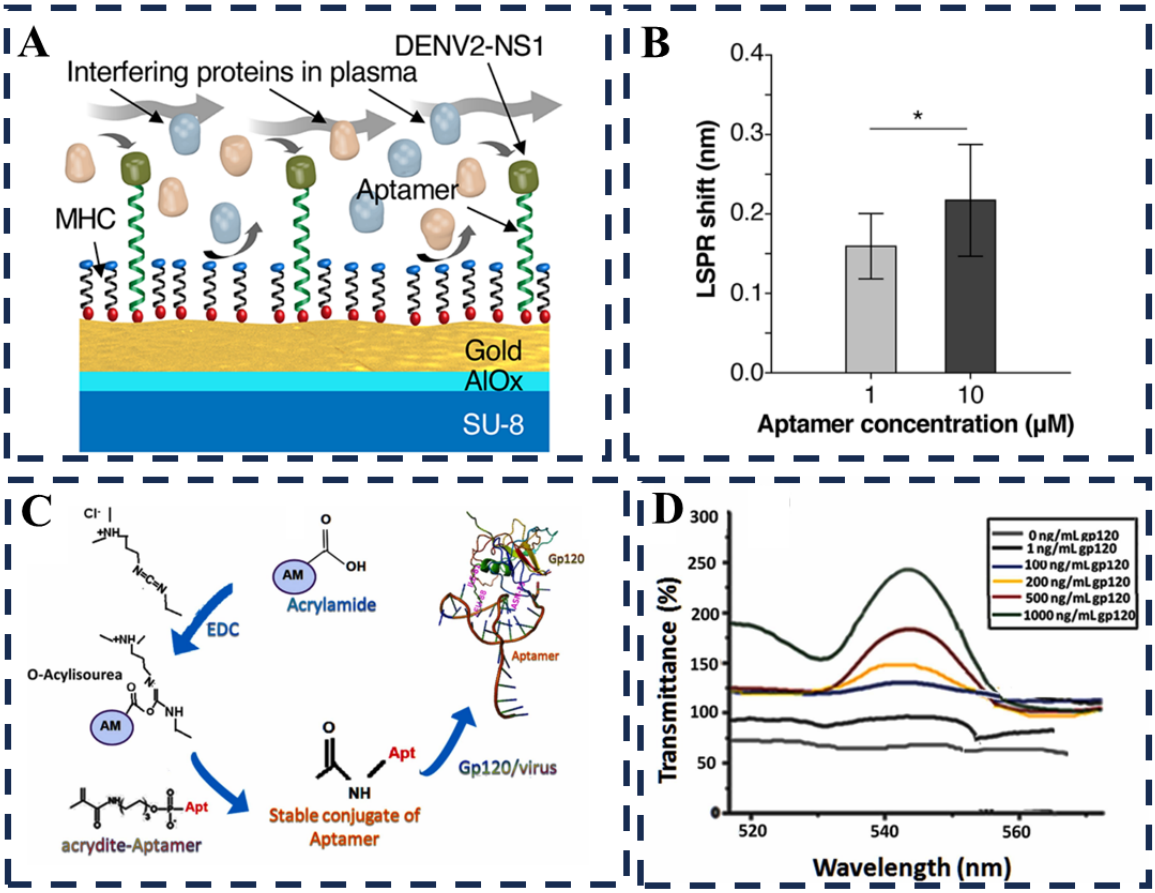

Figure 6. A) Schematic illustration of biological binding of biomarker to the ssDNA aptamer functionalized sensor. B) LSPR shift of the sensor with the increasing aptamer concentration. C) Schematic illustration of the interaction of acrylamide with EDC to form acrydite-aptamer and the molecular docking of aptamer and virus. D) UV-Vis spectra of APC-hydrogel interaction with virus. A,B) Reproduced with permission from ref.[129] Copyright 2021, ACS. C) Reproduced with permission from ref.[130] Copyright 2022, Elsevier. D) Reproduced with permission from ref.[74] Copyright 2023, Elsevier.

4.3 Antibody

Antibodies are the natural biorecognition elements that provide high specificity and affinity in bond with target antigens. The monoclonal antibody (mAbs) can provide sensitive detection, low-cost, fast response time, and simple.[131] A previous study reveal the potency of monoclonal antibody functionalization on SPR-titled fiber Bragg grating (TFBG) to detect Enterovirus A71 (EV-A71). The first step to functionalize SPR-TFBG was to treat it with carboxylic acid and the formation of a self-assembled monolayer (SAM). After that, residual substances were removed from the gold surface then the gold surface was activated by the immersion of 1-ethyl-3-(3-dimethylaminopropyl) carbodiimide (WSC) and N-Hydroxysuccinimide (NHS). The binding of monoclonal antibody with gold surface was then coupled with amine coupling kit,

709 ended with the blocking step, and finally ready for virus test. The performance in SPR mode
710 power indicating the increasing virus concentrations increased the change of SPR mode.[132]

711 The rapid detection of viruses can also be achieved by functionalized whispering gallery mode
712 (WGM) microsphere with polyclonal antibodies. The polyclonal antibodies of influenza A were
713 coated on the WGM microsphere and coupled with an optofluidic platform to detect influenza
714 A viruses. Figure 7A illustrates the mechanism of antibody coated WGM microsphere on
715 micropillar array in the presence of virus samples. The WGM spectra was shifted when the
716 WGM microsphere contact with virus samples. The sensing platform successfully detects the
717 virus in less than 15 minutes and only a few microliters of samples are required.[133]

718 Another study functionalized a gold SPR chip using 4-mercaptobenzoic acid (4-MBA) to
719 immobilize the monoclonal antibody of the recombinant nucleoprotein of Ebola virus (EBOV-
720 rNP).[131] The functionalization process starts from immobilizing 4-MBA on the gold chip using
721 a spin coater then chemically treated with EDC and NHS to activate the carboxylic group of 4-
722 MBA. The activated chip surface is then injected by EBOV-rNP then added with ethanolamine
723 to block the active site. The immobilized sensor surfaces the regenerated by HCl. The
724 interaction of mAb and EBOV-rNP was endothermic and spontaneous interaction. Increasing
725 the concentration of EBOV-rNP was increased the angle of SPR curves. This developed SPR
726 sensor has limit of detection (LOD) 0.5 pg/ml for Ebola virus detection.[131]

727 An immobilization antibody on Au nanoparticles on SPR sensors was also reported to
728 sensitively detect SARS-CoV-2 nucleocapsid protein, as illustrated in Figure 7B. The primary
729 antibody immobilized the Au surface, while the secondary antibody functionalized the Au
730 nanoparticles. The secondary antibody was found to enhance the affinity of the antibody and
731 antigen, leading to an increasing shift in the SPR angle. In addition, the size of the Au
732 nanoparticles affected the sensors' sensitivity; the larger the Au nanoparticles, the greater the
733 SPR shift. The sensor was found to be able to detect SARS-CoV-2 protein with a minimum
734 concentration of 85 fM.[134]

735 The novel monoclonal antibody has been developed to improve the specificity of the SPR
736 sensor in detecting the H7N9 virus. The new monoclonal antibody was produced by
737 immunization of trimeric recombinant hemagglutinin of the H7N9 virus. The preparation step
738 of monoclonal antibody is immunizing the BALB/c mice using trimeric recombinant HA7 (tri-
739 rHA7) with complete Freund’s adjuvant then the mice were boosted by tri-rHA7 proteins that
740 were emulsified by incomplete Freund’s adjuvant. After that, the mice were collected and fused

741 with myeloma cells, diluted, and specific individual antibodies could be obtained. Using this
742 newly generated antibody, the sensor has higher specificity to the H7N9 virus than the other
743 influenza virus as shown in Figure 7C.[135] The new monoclonal antibody is also used to detect
744 SARS-CoV-2 using the phase-sensitive (PS) SPR biosensors. The monoclonal antibodies were
745 produced from recombinant SARS-CoV-2 spike S1 proteins through the conventional
746 hybridoma technique.[136] The binding affinity of anti-S monoclonal antibody with spike S1
747 protein resulted the S-mAb 10-11G can be developed for COVID-19 diagnostics. The S-mAb
748 10-11G can be recognize epitope of SARS-CoV-2 variants (Alpha strain, Beta strain, Delta
749 strain, and Omicron) on its C-terminal of the RBD. The experiment using S-mAb 10-11G also
750 reveal the potency of monoclonal antibody for COVID-19 therapy due to partial neutralization
751 abilities.[136]

752

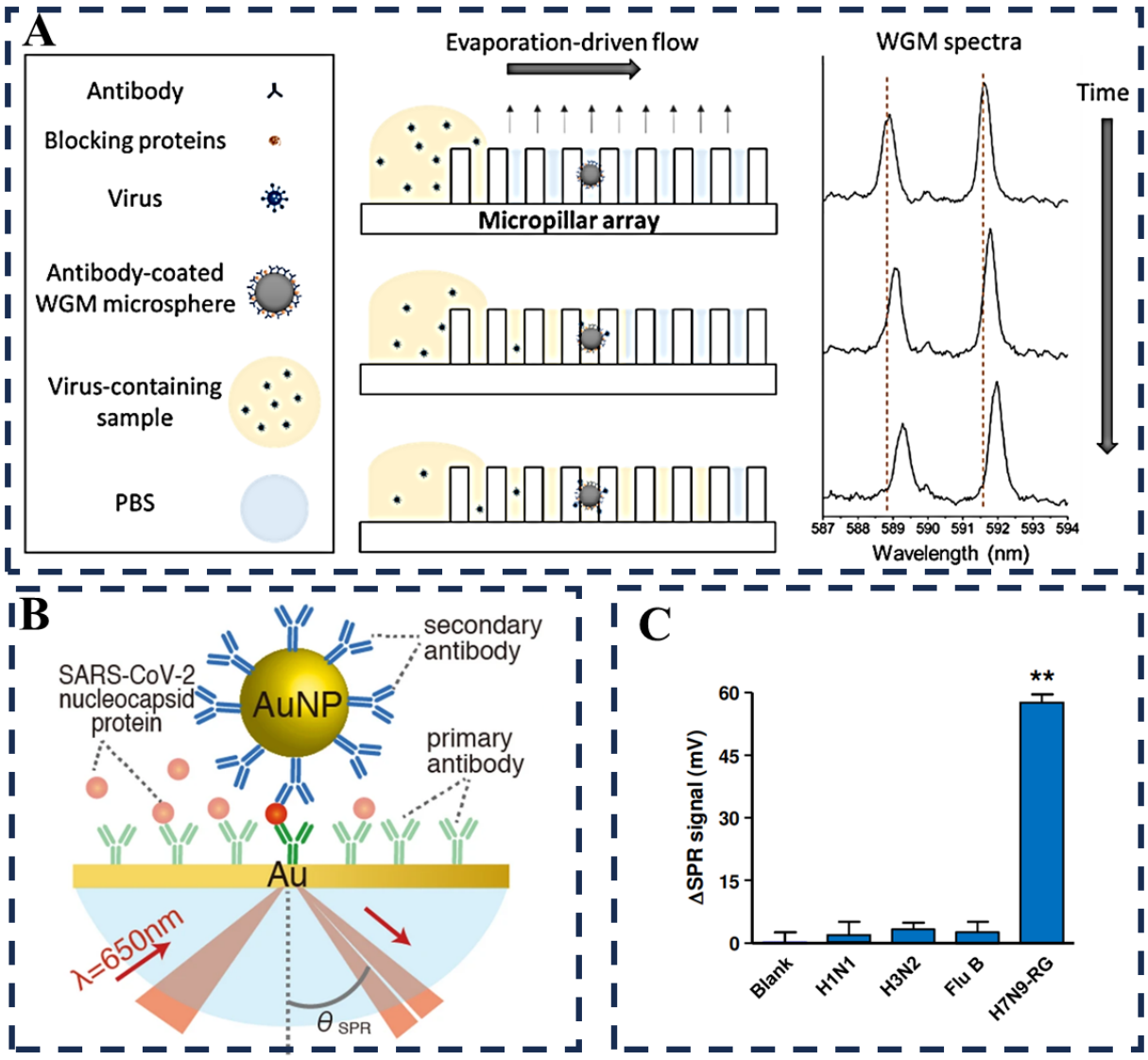

753

754 **Figure 7.** A) Schematic illustration of virus sensing by antibody coated WGM microsphere
755 coupled by optofluidic leading the WGM shifts. B) Illustration of SARS-CoV-2 nucleocapsid
756 protein detection by Au nanoparticles coated with antibody. C) Specificity evaluation of
757 generated monoclonal antibody in detecting human influenza viruses. A) Reproduced with
758 permission from ref.[133] Copyright 2024, ACS. B) Reproduced with permission from ref.[134]
759 Copyright 2022, Springer Nature. C) Reproduced with permission from ref.[135] Copyright 2018,
760 ACS.

761 **5. Outlook**

762 Integration of photonics transducer, materials, and biological receptors was important in
763 developing optical sensors for virus detection to serve high sensitivity, high selectivity, and
764 rapid detection. Table 2 displays the performance of various integration of photonic methods,
765 materials, and biological receptors in virus detection. Although all photonic transducers,

materials, and biological receptors provide advantages in sensor applications, it still has several limitations as summarized in the previous section. In this section, we will provide a multidisciplinary approach for translating photonic biosensors as a future direction for virus detection. As illustrated in Figure 8, the research landscape for photonic biosensors is diverse and expansive.

The selection of the transducer for photonic biosensors is a strategic approach to improve their stability, response time, and sensitivity. Among various photonic detection methodologies, SPR stands out for offering real-time and label-free detection capabilities. SPR sensing signals can be based on four responses, such as intensity, wavelength, angle, and phase, rendering the phase sensitivity more significant than the other signal changes. A pioneering study demonstrated the efficacy of integrating phase-sensitive SPR (PS-SPR) with monoclonal antibodies as the biorecognition element, significantly amplifying the sensor's sensitivity and specificity.[136] The setup of the phase-sensitive SPR sensor is illustrated in Figure 8A. This innovative combination achieved rapid response times (under 10 min) and a low LOD of 11 pg/ml in detecting recombinant SARS-CoV-2 S1 protein.[136] Remarkably, the performance of PS-SPR (589 copies/ml) was found to be on par with qRT-PCR (312 copies/ml) technique in PBS solution, showcasing higher sensitivity compared to ELISA (4000 copies/ml) and SRAT (40000 copies/ml).[136] These findings indicate the potential of leveraging newly synthesized antibodies in conjuction with SPR phase shift, facilitated by simultaneous polarization, as a promising avenue for rapid, highly specific, and sensitive virus detection.

Beside optimizing sensing method of phase or intensity, the promising transduction method in the future through SPR technique is using D-shape fibers.[137] The structure contains two-hexagon-shaped air-hole rings with a small air hole in the center, the diameter of the perfectly matched layer (PML) is 1.71 μm. This unique D-shaped photonic crystal fiber (PCF) structure proposing a conducive upper surface enabling metallic layer deposition.[87] The multilayer PCF-based consist of Au, barium titanate, and graphene has been developed to detect COVID-19 virus using monoclonal antibodies as probe ligand. The performance of the D-shape PCF SPR biosensor was analyze using the finite element method.[137] The wavelength sensitivity of the proposed sensor was 2380 nm/RIU while the amplitude sensitivity was 15.26/RIU.[137] Another experiment also reveal the potency of using D-shape PCF with the structure of PCF consisting of graphene, titanium, and silver. The results demonstrate sensitivity variations in the range of 500–4250 nm/RIU with a wide operating bandwidth, indicating the potential of this structure to detect diverse analytes.[87] This study is exemplary work where the modelling approach could

be used to design and improve the photonic biosensing performances. Other studies have successfully performed numerical analysis of a surface plasmon resonance-based biosensor using a modified D-shaped photonic crystal fiber (DPCF) with a circular air hole design. The illustration of D-shape models can be seen in Figure 8B. The combination of gold (Au) and MXene is applied over the smooth surface of the DPCF. The simulation findings demonstrate that the utilization of MXene with a thickness of up to 27 nm can significantly improve sensitivity by up to 13,000 nm/RIU, representing a 6.5 times enhancement compared to the absence of MXene. Furthermore, we achieved a high sensitivity of 305 RIU^{-1}, a resolution of 1.0×10^{-5} RIU, and a figure of merit of 130 RIU^{-1}. The refractive index (RI) values of this sensor material range from 1.33 to 1.39, suggesting that it can detect biomolecules such as viruses and bacteria.[138]

In terms of material design, the promising material is borophene and graphene as illustrated in Figure 8C. Borophene distinguished by its dimensional diversity ranging from 0 to 3 dimensions and possessing various allotropes, including 2-Pmmn, χ3, honeycomb, and β12, all of which are metallic in nature.[139] The unique structural of borophene imparts several characteristics, such as anisotropic properties, high conductivity, potential surface functionalization, and controllable optical properties.[140] These properties have the potential to enhance the sensitivity and selectivity of photonic biosensors, particularly in detecting biomolecular compounds. The numerical modelling has been successfully conducted to create a layered photonics biosensor based on borophene-$Ge_2Sb_2Te_5$ (GST)-silica-Ag, with the top layer of Ag designed as a grating for the wavelength range of 1.3–1.5 μm. The proposed structure capitalizes on the surface plasmon resonance principle to facilitate detection. Modification to parameters such as material height, grating spacing, wide-angle incidence, and GST material phase, were explored. The study predicts resonance at refractive indices between 1 to 2.5, which corresponds to the refractive indices of biomolecules such as cancer cells, hemoglobin, and saliva.[141] This numerical modelling approach opens up the potential use of borophene in the future experiment laboratory to be used as a supporting material in photonic biosensor applications, especially for detecting biomolecules.

Another promising material to be explored is graphene due to its large surface-to-volume ratio with exceptional optoelectronics properties. Previous studies has been conducted the modelling-based research using graphene-based material for photonic biosensor. The materials utilized include: Aluminum (Al), Gold (Au), Silicon dioxide (SiO_2), Graphene (G), and Gadolinium-Zinc Oxide (GZO). By modifying the thickness of each laminate, the radius of Al

and G, as well as the chemical potential values of each material, testing capabilities were achieved within the wavelength range of 300-600 nm, with a detection sensitivity of ~664.8 nm/RIU, and the ability to detect various strains of the coronavirus. The results of the coronavirus strain variations testing are presented in the UV-Vis graph, where the samples can exhibit distinct spectrum peaks for samples of Avian Fowl Adenovirus (FAdV), Infectious Bronchitis Virus (IBV), Highly Pathogenic Avian Influenza Virus (H5N1 and H5N2), Avian Influenza Virus (H9N2), and Influenza Virus (H4N6).[88] These results indicate that the proposed design materials was promising to detect coronavirus strain variations, and open up the possibility to develop for another virus strain.

In terms of biorecognition elements, DNA origami renowned for its precision in nanoscale assembly, presents a compelling avenue for integration with photonic biosensors. The illustration of DNA origami beacons for biosensing applications is shown in Figure 8D. Using DNA origami with FRET methods, the limit of detection was 100 pM/L for 2 minutes detection times indicating vacinating sensitivity and rapid detection.[125] Under atomic force microscopy (AFM), the nanoscale fluorescence sensor that uses DNA origami technology was shown to have a strong and rigid structure.[120] The architecture of DNA origami enables the specific multivalent interaction and traps electrostatically the virions. Architecturing DNA strand with star-shape was a possess promising candidate due to its detection ability than hexagon, linear, heptagon, and bivalent shapes. The binding of DNA star and aptamer was succsessfully detect DENV with LOD 1000 p.f.u/ml and sensitivity of 100 p.f.u/ml.[124] The ability of the DNA star in developing sensor with high sensitivity opened up the idea of the future to detect biomolecules based on DNA origami technology. In addition, the DNA origami with the structure of 4x4 DNA Net also possesses the possibility to develop as a virus sensor in the future due to its direct interaction with a virus, simplify the complex sample preparation, affordable cost, and provide therapeutic potency.

Furthermore, antibodies serve as another vital biorecognition elements, particularly for virus detection application. Several research has been conducted to conjugate the monoclonal antibody with sensor systems to provide better performance of viral recognition.[138] Monoclonal antibodies can increase the response time, sensitivity, and specificity of the sensor systems.[131] As illustrated in Figure 8E, the monoclonal antibody can be covalently immobilized on the SPR chip to detect the H7N9-RG virus.[135] The integration of monoclonal antibodies with SPR sensing methods serves as a highly specific recognizer of influenza virus

with a fast detection time (less than 10 minutes) indicating its potency in the future to detect another virus strain.

Furthermore, enzymes also possess potential as natural biorecognition elements for photonics sensor. The high catalytic activity of enzymes allows them to be used in sensor applications to improve signal enhancement.[142] In terms of SARS-CoV-2, angiotensin-converting enzyme-2 (ACE-2).[143] ACE-2 was an important enzyme in the recognition of SARS-CoV-2 because it was the main enzyme to enter human cells. For example, human-ACE-2(hACE2) has been used as a recognition element for detecting SARS-CoV-2 in human saliva. The hACE2 was immobilized by streptavidin-biotin with the target of S protein on UV-attenuated virus.[144] The ACE2-based biosensor can detect S1 mutants of SARS-CoV-2 variants such as alpha and beta variants. It also shows the ability to detect neutralizing antibodies specific for SARS-CoV-2.[145]

Although point-of-care photonic biosensors are currently in the early stage, experts are already envisioning their promising future. The integration system of biosensor and microfluidic holds significant potential for point-of-care diagnostics, offering advantages such as portability, inexpensive device, simplicity to use, rapid detection capabilities, and only needs small quantities of samples and reagents.[127] The development of new material architecture, coupled with the strategic functionalization of biological receptor and photonic method enhancement, present a viable strategy for engineering photonic biosensor that boast ultra-high sensitivity, rapid detection, and high selectivity.

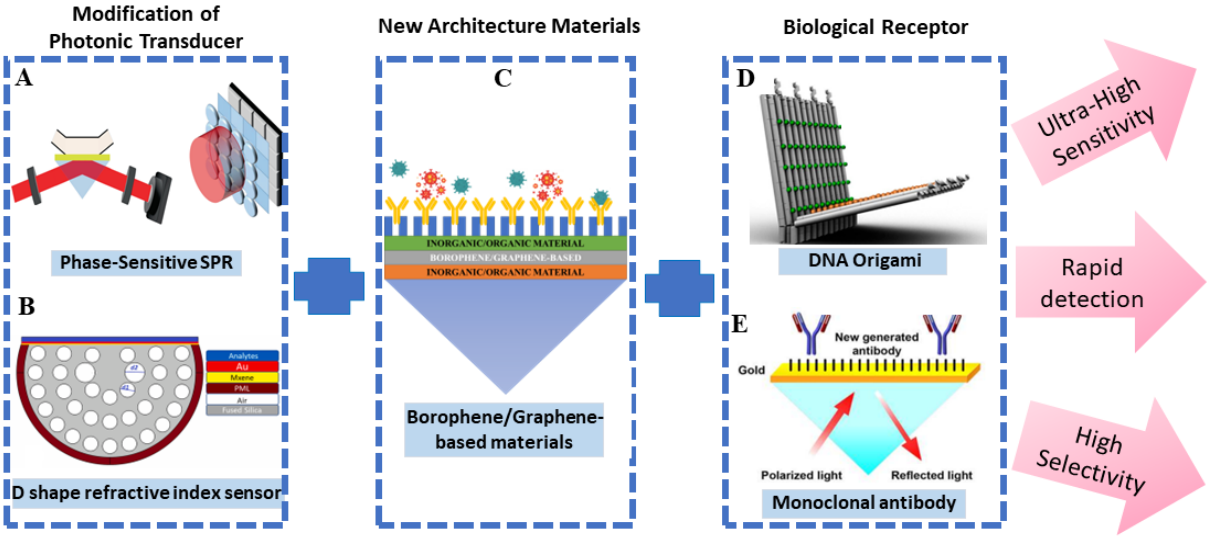

Figure 8. Research outlook of architecture materials, biological receptor, and photonic methods modification in developing ultra-highly sensitive, rapid detection, and high selectivity photonic sensor for virus detection. A) Reproduced with permission from ref.[136] Copyright 2023, Wiley

887 Periodicals LLC. B) Reproduced with permission from ref.[138] Copyright 2022, Elsevier. D)
888 Reproduced with permission from ref.[125] Copyright 2018, ACS Nano. E) Reproduced with
889 permission from ref.[135] Copyright 2018, ACS.

890 **Table 2** Performance of various photonic methods, materials, and biorecognition molecules
891 for virus detection

Method	Materials	Biorecognition molecules	Target analyte	Sensitivity	Selectivity	Rapid Detection	Ref
Intensity-modulated SPR	Ag/Au chips	Monoclonal antibody	H7N9 virus	144 copies/ml	Yes	< 10 min	[135]
Phase-sensitive SPR	Carboxymethyl-dextran CM5 chip	Anti-S monoclonal antibody	SARS-CoV-2 pseudovirus	589 copies/ml	Yes	< 10 min	[136]
Titled fiber Bragg grating (TFBG)-based SPR	Gold-coated fiber	Monoclonal antibody	Enterovirus A71	0.343 µg/ml	Yes	n.a	[132]
SPR	Gold-based chip	Anti-H9N2 antibody	H9N2 virus	6.3 copies/mL	Yes	<10 min	[146]
SPR	Hemicylindrical glass prism-gold-coated glass slide	Antibody	SARS-CoV-2	4 pg/mL	n.a	15 min	[136]
WGM	Self-assembled silica microsphere	Antigen	SARS-CoV-2	500 nm/RIU	Yes	n.a	[147]
WGM-microfluidic platform	Polystyrene microspheres	Polyclonal antibodies	Influenza A	n.a	Yes	15 min	[133]
Photonic crystal (PC)	Cycloolefin polymer-based	antibody	SARS-CoV-2	429 fg/ml	Yes	<15 min	[148]

	imprinted PC film						
Photonic crystal	Polystyrene nanoparticles-polyacrylamide hydrogel	Aptamer	SARS-CoV-2	3 cells/ml	Yes	5 min	[46]

6. Conclusions

The current golden standard to detect SARS-CoV-2 is using RT-PCR, which provides specific and sensitive detection of viral RNA copies. Still, it requires trained operators, high costs, and long processing time. Photonic biosensors have escalated as one candidate that has rapidly developed for virus detection, providing high sensitivity and being relatively easy to miniaturize. One of the promising methods in photonic biosensing is surface plasmon resonance, with several modifications to increase its performance. Another strategy to improve sensor performance was choosing the materials with the preferable characteristics for virus detection. Graphene and borophene-based materials can be a candidate for future materials because of their excellent optical characteristics. Functionalizing and choosing biorecognition molecules were also crucial to increasing the analyte attachment. The integration of photonic methods, materials, and biorecognition elements enables the development of point-of-care diagnostics with high sensitivity, fast responses, and high selectivity.

Acknowledgments

A.W. would like to acknowledge the ITB Research Fund 2023 scheme from the Institut Teknologi Bandung (PN-6-02-2023). A.T. acknowledges the Indonesian Endowment Fund for Education (LPDP) for doctoral scholarship (SKPB-5119/LPDP/LPDP.3/2023). Authors would like to thanks to Dr. Glen Cooper from the University of Manchester for the proofreading of this manuscript.

Received: ((will be filled in by the editorial staff))
Revised: ((will be filled in by the editorial staff))
Published online: ((will be filled in by the editorial staff))

References

[1] C. Menard-Moyon, A. Bianco, K. Kalantar-Zadeh, *ACS Sens.* **2020**, *5*, 3739.
[2] S. Chatterjee, M. Bhattacharya, S. Nag, K. Dhama, C. Chakraborty, *Viruses* **2023**, *15*, 167.

[3] L. Bubba, E. K. Broberg, A. Jasir, P. Simmonds, H. Harvala, M. R. Fritz, L. K. Glomb, M. Havlíčková, P. Rainetova, T. K. Fischer, S. E. Midgley, J. Epštein, S. Blomqvist, S. Böttcher, K. Keeren, E. Bujaki, A. Farkas, G. E. Baldvinsdóttir, U. Morley, C. D. Gascun, L. Pellegrinelli, A. Piralla, O. Martiņuka, N. Zamjatina, A. Griškevičius, T. Nguyen, S. G. Dudman, S. Numanovic, M. Wieczorek, R. Guiomar, I. Costa, C. Tecu, S. Bopegamage, K. Pastuchova, N. Berginc, M. Cabrerizo, R. G. Sanz, K. Zakikhany, E. Hauzenberger, K. Benschop, E. Duizer, J. Dunning, C. Celma, J. McKenna, S. Feeney, K. Templeton, C. Moore, S. Cottrell, *Lancet Infect Dis.* **2020**, *20*, 350.

[4] H. Chen, J. Guo, C. Wang, F. Luo, X. Yu, W. Zhang, J. Li, D. Zhao, D. Xu, Q. Gong, J. Liao, H. Yang, W. Hou, Y. Zhang, *Lancet* **2020**, *395*, 10226.

[5] M. Roberts, D. Driggs, M. Thorpe, J. Gilbey, M. Yeung, S. Ursprung, A. I. A. Rivero, C. Etmann, C. McCague, L. Beer, J. R. W. McCall, Z. Teng, E. G. Klotsas, A. Ruggiero, A. Korhonen, E. Jefferson, E. Ako, G. Langs, G. Gozaliasl, G. Yang, H. Prosch, J. Preller, J. Stanczuk, J. Tang, J. Hofmanninger, J. Babar, L. E. Sánchez, M. Thillai, P. M. Gonzalez, P. Teare, X. Zhu, M. Patel, C. Cafolla, H. Azadbakht, J. Jacob, J. Lowe, K. Zhang, K. Bradley, M. Wassin, M. Holzer, K. Ji, M. D. Ortet, T. Ai, N. Walton, P. Lio, S. Stranks, T. Shadbahr, W. Lin, Y. Zha, Z. Niu, J. H. F. Rudd, E. Sala, C. B. Schönlieb, *Nat. Mach. Intell* **2021**, *3*, 199.

[6] V. Kukushkin, O. Ambartsumyan, A. Astrakhantseva, V. Gushchin, A. Nikonova, A. Dorofeeva, V. Zverev, A. Gambaryan, D. Tikhonova, T. Sovetnikov, A. Akhmetova, I. Yaminsky, E. Zavyalova, *Nanomaterials* **2022**, *12*, 3854.

[7] R. Wang, B. Zhu, P. Young, Y. Luo, J. Taylor, A. J. Cameron, C. J. Squire, J. T. Sejdic, *Biosensors* **2024**, *14*, 10.

[8] R. Liu, L. He, Y. Hu, Z. Luo, J. Zhang, *Chem. Sci.* **2020**, *11*, 12157.

[9] A. Scohy, A. Anantharajah, M. Bodéus, B. K. Mukadi, A. Verroken, H. R. Villalobos, *J. Clin. Virol.* **2020**, *129*, 104455.

[10] A. Singanayagam, M. Patel, A. Charlett, J. Lopez Bernal, V. Saliba, J. Ellis, S. Ladhani, M. Zambon, R. Gopal, *Euro Surveill* **2020**, *25*, 2001483.

[11] V. Singh, K. M. Batoo, M. Singh, *Appl. Phys. A* **2021**, *127*, 960.

[12] J. Wu, X. Liu, D. Zhou, G. Qiu, M. Dai, Q. Yang, Z. Pan, N. Zhou, P. Wu, *Front Public Health* **2020**, *8*, 267.

[13] S. B. Nanjunda, V. N. Seshadri, C. Krishnan, S. Rath, S. Arunagiri, Q. Bao, K. Helmerson, H. Zhang, R. Jain, A. Sundarrajan, B. Srinivasan, **2022**, *11*, 5041.

[14] X. Hao, J. P. St-Pierre, S. Zou, X. Cao, *Biosensors and Bioelectronics* **2023**, *236*, 115421.

[15] G. Gumilar, N. L. W. Septiani, S. Wustoni, T. R. Tohari, W. Widayat, M. Yusuf, H. L. Wiraswati, L. Faridah, S. Ekawardhani, I. Anshori, B. Yuliarto, *J. Ind. Eng. Chem.* **2023**, *127*, 467.

[16] S. Chang, L. Liu, C. Mu, F. Wen, J. Xiang, K. Zhai, B. Wang, L. Wu, A. Nie, Y. Shu, T. Xue, Z. Liu, *J. Colloid Interface Sci.* **2023**, *651*, 938.

[17] T. B. A. Akib, M. M. Rana, I. M. Mehedi, *Biosens. Bioelectron.: X* **2024**, *16*, 100434.

[18] M. El-assar, T. E. Taha, F. E. A. El-Samie, H. A. Fayed, M. H. Aly, *Opt. Quantum Electron.* **2023**, *55*, 1143.

[19] S. Jiang, S. Qian, S. Zhu, J. Lu, Y. Hu, C. Zhang, Y. Geng, X. Chen, Y. Guo, Z. Chen, J. Pu, Z. Guo, S. Liu, *Biosensors* **2023**, *13*, 1029.

[20] J. S. Cognetti, D. J. Steiner, M. Abedin, M. R. Bryan, C. Shanahan, N. Tokranova, E. Young, A. M. Klose, A. Zavriyev, N. Judy, B. Piorek, C. Meinhart, R. Jakubowicz, H. Warren, N. C. Cady, B. L. Miller, *Lab Chip* **2021**, *21*, 2913.

[21] B. Uttara, N. Chittaranjan, R. J. Kumar, *Opt. Eng.* **2022**, *62*, 010901.

[22] S. M. Neher, J. Spinke, M. Liley, G. Nelles, M. Weisser, R. Back, G. Wenz, W. Knoll, *Biosensors and Bioelectronics* **1995**, *10*, 903.

[23] M. E. Stewart, C. R. Anderton, L. B. Thompson, J. Maria, S. K. Gray, J. A. Rogers, R. G. Nuzzo, *Chem Rev* **2008**, *108*, 494.

[24] N. Skivesen, A. Têtu, M. Kristensen, J. Kjems, L. H. Frandsen, P. I. Borel, *Opt. Express* **2007**, *15*, 3169.

[25] E. Petryayeva, W. R. Algar, I. L. Medintz, *Appl Spectrosc* **2013**, *67*, 215.

[26] J. Ge, Y. Yin, *Angew. Chem., Int. Ed.* **2011**, *50*, 1492.

[27] H. Inan, M. Poyraz, F. Inci, M. A. Lifson, M. Baday, B. T. Cunningham, U. Demirci, *Chem. Soc. Rev.* **2017**, *46*, 366.

[28] G. Pitruzzello, T. F. Krauss, *J. Opt.* **2018**, *20*, 073004.

[29] A. A. Rifat, R. Ahmed, A. K. Yetisen, H. Butt, A. Sabouri, G. A. Mahdiraji, S. H. Yun, F. R. M. Adikan, *Sens. Actuators, B* **2017**, *243*, 311.

[30] B. Kaur, S. Kumar, B. K. Kaushik, *Biosens Bioelectron* **2022**, *197*, 113805.

[31] A. Shafkat, A. N. Z. Rashed, H. M. El-Hageen, A. M. Alatwi, *J. Sol-Gel Sci. Technol.* **2021**, *98*, 202.

[32] V. S. Chaudhary, D. Kumar, S. Kumar, *IEEE Sens. J.* **2021**, *21*, 17800.

[33] A. Yasli, *Plasmonics* **2021**, *16*, 1605.

[34] H. Altug, S. H. Oh, S. A. Maier, J. Homola, *Nat. Nanotechnol.* **2022**, *17*, 5.

[35] S. L. Lee, J. Kim, S. Choi, J. Han, G. Seo, Y. W. Lee, *Talanta* **2021**, *235*, 122801.

[36] X. Han, H. Zhong, K. Li, X. Xue, W. Wu, N. Hu, X. Lu, J. Huang, G. Xiao, Y. Mai, T. Guo, *Light: Sci. Appl.* **2024**, *13*, 24.

[37] Q. Chen, S. Wang, T. Huang, F. Xiao, Z. Wu, R. Yu, *Anal. Chem.* **2022**, *94*, 5530.

[38] M. A. Butt, S. N. Khonina, N. L. Kazanskiy, *Opt. Laser Technol.* **2021**, *142*, 107265.

[39] V. Bello, W. Vandezande, D. Daems, J. Lammertyn, *ACS Sens.* **2022**, *7*, 3360.

[40] Z. H. Lin, S. Kushida, F. C. Lin, J. Y. Chen, A. K. Singh, Y. Yamamoto, J. S. Huang, *Nano Lett.* **2023**, *23*, 6512.

[41] T. Watabe, K. Terai, K. Sumiyama, M. Matsuda, *ACS Sens.* **2020**, *5*, 719.

[42] J. Chen, W. K. H. Ho, B. Yin, Q. Zhang, C. Li, J. Yan, Y. Huang, J. Hao, C. Yi, Y. Zhang, S. H. D. Wong, M. Yang, *Biosensors and Bioelectronics* **2024**, *248*, 115969.

[43] W. Liu, H. Ma, A. Walsh, *Renewable Sustainable Energy Rev.* **2019**, *116*, 109436.

[44] D. Chen, L. Huo, H. Li, G. Song, *Sens.* **2018**, *18*, 2586.

[45] P. Shen, Y. Zhang, Z. Cai, R. Liu, X. Xu, R. Li, J. J. Wang, D. Yang, *J. Mater. Chem. C* **2021**, *9*, 5840.

[46] G. Murtaza, A. S. Rizvi, M. Xue, L. Qiu, Z. Meng, *Anal. Chem.* **2022**, *94*, 7391.

[47] J. Liu, M. Nero, K. Jansson, T. Willhammar, M. H. Sipponen, *Nat. Commun.* **2023**, *14*, 3099.

[48] P. R. Miller, R. J. Narayan, R. Polsky, *J. Mater. Chem. B* **2016**, *4*, 1379.

[49] J. Qin, X. Li, L. Cao, S. Du, W. Wang, S. Q. Yao, *J. Am. Chem. Soc.* **2020**, *142*, 417.

[50] S. Pan, M. Xia, H. Li, X. Jiang, P. He, Z. Sun, Y. Zhang, *J. Mater. Chem. C* **2020**, *8*, 2827.

[51] J. Zhao, X. Cai, X. Zhang, J. Zhang, J. Fan, F. Ma, W. Zhu, X. Jia, S. Wang, Z. Meng, *ACS Appl. Mater. Interfaces* **2023**, *15*,

[52] Y. Meng, J. Feng, S. Han, Z. Xu, W. Mao, T. Zhang, J. S. Kim, I. Roh, Y. Zhao, D. H. Kim, Y. Yang, J. W. Lee, L. Yang, C. W. Qiu, S. H. Bae, *Nat. Rev. Mater.* **2023**, *8*, 498.

[53] J. Wang, Z. Xu, D. G. Kotsifaki, *Sens. Diagn.* **2023**, *2*, 600.

[54] M. Raynaud, A. Héron, J. C. Adam, *Sci. Rep.* **2020**, *10*, 13450.

[55] A. Kumar, A. Kumar, S. K. Srivastava, *Plasmonics* **2022**, *17*, 1065.

[56] H. Xin, B. Namgung, L. P. Lee, *Nat. Rev. Mater.* **2018**, *3*, 228.

[57] O. Tokel, F. Inci, U. Demirci, *Chem. Rev.* **2014**, *114*, 5728.

[58] K. Bi, Y. Chen, Q. Wan, T. Ye, Q. Xiang, M. Zheng, X. Wang, Q. Liu, G. Zhang, Y. Li, Y. Liu, H. Duan, *Nanoscale* **2019**, *11*, 1245.

[59] W. G. Kim, J. M. Lee, Y. Yang, H. Kim, V. Devaraj, M. Kim, H. Jeong, E. J. Choi, J. Yang, Y. Jang, T. Badloe, D. Lee, J. Rho, J. T. Kim, J. W. Oh, *Nano Lett.* **2022**, *22*, 4702.
[60] L. K. Chin, J. Y. Yang, B. Chousterman, S. Jung, D. G. Kim, D. H. Kim, S. Lee, C. M. Castro, R. Weissleder, S. G. Park, H. Im, *ACS Nano* **2023**, *17*, 3610.
[61] F. Vollmer, S. Arnold, *Nat. Methods* **2008**, *5*, 591.
[62] E. Yacoby, Y. Meshorer, Y. London, *Opt. Laser Technol.* **2022**, *151*, 108019.
[63] Y. Lv, X. Xiong, Y. Liu, J. Yao, Y. J. Li, Y. S. Zhao, *Nano Lett.* **2019**, *19*, 1098.
[64] N. Bavili, T. Balkan, B. Morova, M. Eryürek, Y. Uysallı, S. Kaya, A. Kiraz, *Sens. Actuators, B* **2020**, *310*, 127806.
[65] E. Ozgur, K. E. Roberts, E. O. Ozgur, A. N. Gin, J. R. Bankhead, Z. Wang, J. Su, *Anal. Chem.* **2019**, *91*, 11872.
[66] X. Jiang, L. Yang, *Light: Sci. Appl.* **2020**, *9*, 24.
[67] N. Toropov, G. Cabello, M. P. Serrano, R. R. Gutha, M. Rafti, F. Vollmer, *Light: Sci. Appl.* **2021**, *10*, 42.
[68] X. Jiang, L. Shao, S. X. Zhang, X. Yi, J. Wiersig, L. Wang, Q. Gong, M. Lončar, L. Yang, Y. F. Xiao, *Sci.* **2017**, *358*, 6361.
[69] W. Mao, Y. Li, X. Jiang, Z. Liu, L. Yang, *Light: Sci. Appl.* **2023**, *12*, 247.
[70] W. R. Algar, N. Hildebrandt, S. S. Vogel, I. L. Medintz, *Nat. Methods* **2019**, *16*, 815.
[71] X. Lao, Y. Liu, L. Li, M. Song, Y. Ma, M. Yang, G. Chen, J. Hao, *Aggregate* **2023**, *5*, e448.
[72] M. Ouyang, R. Wan, Q. Qin, Q. Peng, P. Wang, J. Wu, M. Allen, Y. Shi, S. Laub, L. Deng, S. Lu, Y. Wang, *ACS Sens.* **2019**, *4*, 76.
[73] T. Chen, H. Pham, A. Mohamadi, L. W. Miller, *iScience* **2020**, *23*, 101533.
[74] A. S. Rizvi, G. Murtaza, W. Zhang, M. Xue, L. Qiu, Z. Meng, *J. Pharm. Biomed. Anal.* **2023**, *227*, 115104.
[75] G. Konoplev, D. Agafonova, L. Bakhchova, N. Mukhin, M. Kurachkina, M. P. Schmidt, N. Verlov, A. Sidorov, A. Oseev, O. Stepanova, A. Kozyrev, A. Dmitriev, S. Hirsch, *Biomed.* **2022**, *10*, 207.
[76] W. Liu, Y. Wang, X. Han, P. Lu, L. Zhu, C. Sun, J. Qian, S. He, *Nanoscale* **2018**, *10*, 10025.
[77] O. Hosu, A. Florea, C. Cristea, R. Sandulescu, "Chapter 6 - Functionalized Advanced Hybrid Materials for Biosensing Applications," in *Advanced Biosensors for Health Care Applications*, Inamuddin, R. Khan, A. Mohammad, and A. M. Asiri Eds. Cluj-Napoca, Romania: Elsevier, 2019, ch. 6, pp. 171-207.
[78] K. Saha, S. S. Agasti, C. Kim, X. Li, V. M. Rotello, *Chem. Rev.* **2012**, *112*, 2739.
[79] S. Chakma, M. A. Khalek, B. K. Paul, K. Ahmed, M. R. Hasan, A. N. Bahar, *Sens. Bio-Sens. Res.* **2018**, *18*, 7.
[80] K. V. Sreekanth, Q. Ouyang, S. Sreejith, S. Zeng, W. Lishu, E. Ilker, W. Dong, M. ElKabbash, Y. Ting, C. T. Lim, M. Hinczewski, G. Strangi, K. T. Yong, R. E. Simpson, R. Singh, *Adv. Opt. Mater.* **2019**, *7*, 190081
[81] G. Qiu, Z. Gai, Y. Tao, J. Schmitt, G. A. K. Ublick, J. Wang, *ACS Nano* **2020**, *14*, 5268.
[82] S. Zhu, R. Jaffiol, A. Crunteanu, C. Vézy, S. T. Chan, W. Yuan, H. P. Ho, S. Zeng, *Light: Sci. Appl.* **2024**, *13*, 106728.
[83] S. Khani, M. Hayati, *Sci. Rep.* **2022**, *12*, 5246.
[84] H. Lu, J. Zhu, J. Chen, T. Tao, Y. Shen, H. Zhou, *Talanta* **2024**, *272*, 125773.
[85] Y. E. Monfared, M. Qasymeh, *Plasmonics* **2021**, *16*, 881.
[86] I. J. Budiarso, V. A. Dabur, R. Rachmantyo, H. Judawisastra, C. Hu, A. Wibowo, *Mater. Adv.* **2024**, 2668.

[87] V. Sorathiya, S. Lavadiya, O. S. Faragallah, M. M. A. Eid, A. N. Z. Rashed, *Opt. Quantum Electron.* **2022**, *54*, 290.

[88] R. Negahdari, E. Rafiee, Z. Kordrostami, *Plasmonics* **2023**, *18*, 1325.

[89] E. Lizundia, T. D. Nguyen, R. J. Winnick, M. J. MacLachlan, *J. Mater. Chem. C* **2021**, *9*, 796.

[90] V. V. V. Neuling, M. Saba, I. Gunkel, J. O. Zoppe, U. Steiner, B. D. Wilts, A. Dodero, *Adv. Funct. Mater.* **2023**, *n/a*, 2306528.

[91] A. P. C. Almeida, J. P. Canejo, S. N. Fernandes, C. Echeverria, P. L. Almeida, M. H. Godinho, *Adv. Mater.* **2018**, *30*, 1703655.

[92] R. M. Parker, T. G. Parton, C. L. C. Chan, M. M. Bay, B. F. Petesic, S. Vignolini, *Acc. Mater. Res.* **2023**, *4*, 522.

[93] P. C. Nath, R. Sharma, S. Debnath, M. Sharma, B. S. Inbaraj, P. K. Dikkala, P. K. Nayak, K. Sridhar, *Int. J. Biol. Macromol.* **2023**, *253*, 127524.

[94] G. Ge, Y. Zhang, J. Shao, W. Wang, W. Si, W. Huang, X. Dong, *Adv. Funct. Mater.* **2018**, *28*, 1802576.

[95] Z. Lei, Q. Wang, S. Sun, W. Zhu, P. Wu, *Adv. Mater.* **2017**, *29*, 1700321.

[96] M. Ramuz, B. C. K. Tee, J. B. H. Tok, Z. Bao, *Adv. Mater.* **2012**, *24*, 3223.

[97] X. Wang, Y. Wang, C. Lu, J. Zhang, W. Qiu, S. Yang, N. Lin, Y. Zhang, X. Y. Liu, *Cell Rep. Phys. Sci.* **2023**, *4*, 101490.

[98] R. M. Parker, G. Guidetti, C. A. Williams, T. Zhao, A. Narkevicius, S. Vignolini, B. F. Petesic, *Adv. Mater.* **2018**, *30*, 1704477.

[99] C. Duan, Z. Cheng, B. Wang, J. Zeng, J. Xu, J. Li, W. Gao, K. Chen, *Small* **2021**, *17*, 2007306.

[100] K. Uetani, H. Koga, M. Nogi, *ACS Macro Lett.* **2019**, *8*, 250.

[101] L. Huang, X. Zhang, L. Deng, Y. Wang, Y. Liu, H. Zhu, *ACS Nano* **2024**, *18*, 3627.

[102] D. Knorr, *Food Technol.* **1984**, *38*, 85.

[103] M. Ibrahim, O. Osman, A. Mahmoud, *J. Comput. Theor. Nanosci.* **2011**, *8*, 117.

[104] P. S. Bakshi, D. Selvakumar, K. Kadirvelu, N. S. Kumar, *Int. J. Biol. Macromol.* **2020**, *150*, 1072.

[105] I. J. Budiarso, N. D. W. Rini, A. Tsalsabila, M. D. Birowosuto, A. Wibowo, *ACS Biomater. Sci. Eng.* **2023**, *9*, 3084.

[106] T. C. Lin, C. Y. Yang, T. L. Lee, J. W. Lin, Y. T. Liang, Y. T. Xie, Z. H. Xie, Y. C. Hung, R. M. Ho, *NPG Asia Mater.* **2023**, *15*, 13.

[107] R. Ravikumar, L. H. Chen, M. M. X. Hui, C. C. Chan, *J. Lightwave Technol.* **2019**, *37*, 2778.

[108] G. Huang, Y. Yin, Z. Pan, M. Chen, L. Zhang, Y. Liu, Y. Zhang, J. Gao, *Biomacromolecules* **2014**, *15*, 4396.

[109] H. Wang, L. Ma, Z. Jin, Z. Cui, H. Yang, M. Miao, *Talanta* **2023**, *257*, 124360.

[110] S. Li, Z. Wang, Y. Chen, Q. Zou, Q. Zou, L. Wang, Y. Zhu, L. Wang, *RSC Adv.* **2023**, *13*, 18363.

[111] S. T. Wu, F. Yang, C. Q. Zhao, L. D. Xu, X. L. Han, P. Chen, S. N. Ding, *Dyes Pigm.* **2022**, *199*, 110089.

[112] K. M. Al-Qaoud, Y. M. Obeidat, T. Al-Omari, M. Okour, M. M. Al-Omari, M. I. Ahmad, R. Alshadfan, A. M. M. Rawashdeh, *Sci. Rep.* **2024**, *14*, 748.

[113] M. Alafeef, K. Dighe, P. Moitra, D. Pan, *ACS Nano* **2020**, *14*, 17028.

[114] J. Escorihuela, M. J. Bañuls, J. G. Castelló, V. Toccafondo, J. García-Rupérez, R. Puchades, Á. Maquieira, *Anal. Bioanal. Chem.* **2012**, *404*, 2831.

[115] H. Shafiee, E. A. Lidstone, M. Jahangir, F. Inci, E. Hanhauser, T. J. Henrich, D. R. Kuritzkes, B. T. Cunningham, U. Demirci, *Sci Rep* **2014**, *4*, 4116.

[116] Q. Ouyang, S. Zeng, L. Jiang, L. Hong, G. Xu, X. Q. Dinh, J. Qian, S. He, J. Qu, P. Coquet, K. T. Yong, *Sci Rep* **2016**, *6*, 28190.

[117] M. Lu, *Viruses* **2021**, *13*, 332.
[118] Y. Wang, Y. Zhang, J. Chen, M. Wang, T. Zhang, W. Luo, Y. Li, Y. Wu, B. Zeng, K. Zhang, R. Deng, W. Li, *Anal. Chem.* **2021**, *93*, 3393.
[119] C. Shen, Z. Huang, X. Chen, Z. Wang, J. Zhou, Z. Wang, D. Liu, C. Li, T. Zhao, Y. Zhang, S. Xu, W. Zhou, W. Peng, *Biosensors and Bioelectronics* **2023**, *242*, 115719.
[120] L. Yang, Z. Zhang, R. Zhang, H. Du, T. Zhou, X. Wang, F. Wang, *J. Photochem. Photobiol., A* **2023**, *438*, 114515.
[121] L. G. Gálvez, D. G. Fernández, M. Barrio, M. Luna, I. Torres, F. Zamora, C. Navío, P. M. Rois, M. Castellanos, M. Abreu, R. Cantón, J. C. Galán, A. Somoza, R. Miranda, T. G. Mendiola, E. Lorenzo, *Talanta* **2024**, *269*, 125405.
[122] P. Williamson, P. Piskunen, H. Ijäs, A. Butterworth, V. Linko, D. K. Corrigan, *ACS Sens.* **2023**, *8*, 1471.
[123] N. Chauhan, Y. Xiong, S. Ren, A. Dwivedy, N. Magazine, L. Zhou, X. Jin, T. Zhang, B. T. Cunningham, S. Yao, W. Huang, X. Wang, *J. Am. Chem. Soc.* **2023**, *145*, 20214.
[124] P. S. Kwon, S. Ren, S. J. Kwon, M. E. Kizer, L. Kuo, M. Xie, D. Zhu, F. Zhou, F. Zhang, D. Kim, K. Fraser, L. D. Kramer, N. C. Seeman, J. S. Dordick, R. J. Linhardt, J. Chao, X. Wang, *Nat. Chem.* **2020**, *12*, 26.
[125] D. Selnihhin, S. M. Sparvath, S. Preus, V. Birkedal, E. S. Andersen, *ACS Nano* **2018**, *12*, 5699.
[126] X. Zhao, Z. Zhu, R. Zou, L. Wang, H. Gong, C. Cai, *Microchem. J.* **2021**, *170*, 42046.
[127] T. C. Chang, A. Y. Sun, Y. C. Huang, C. H. Wang, S. C. Wang, L. K. Chau, *Biosensors* **2022**, *12*, 785.
[128] R. Sun, Y. Zhou, Y. Fang, Y. Qin, Y. Zheng, L. Jiang, *Anal. Bioanal. Chem.* **2024**, *416*, 1667.
[129] A. Vazquez-Guardado, F. Mehta, B. Jimenez, A. Biswas, K. Ray, A. Baksh, S. Lee, N. Saraf, S. Seal, D. Chanda, *Nano Lett.* **2021**, *21*, 7505.
[130] M. Adeel, K. Asif, F. Alshabouna, V. Canzonieri, M. M. Rahman, S. A. Ansari, F. Güder, F. Rizzolio, S. Daniele, *Biosens. Bioelectron.: X* **2022**, *12*, 100256.
[131] P. K. Sharma, J. S. Kumar, V. V. Singh, U. Biswas, S. S. Sarkar, S. I. Alam, P. K. Dash, M. Boopathi, K. Ganesan, R. Jain, *Anal. Bioanal. Chem.* **2020**, *412*, 4101.
[132] W. Udos, C. W. Ooi, S. H. Tan, K. S. Lim, Y. J. Ee, K. C. Ong, H. Ahmad, *Optik* **2021**, *228*, 166221.
[133] B. Guan, T. W. Kok, N. Riesen, D. Lancaster, K. Suu, C. Priest, *ACS Appl. Mater. Interfaces* **2024**, *16*, 12042.
[134] T. A. Yano, T. Kajisa, M. Ono, Y. Miyasaka, Y. Hasegawa, A. Saito, K. Otsuka, A. Sakane, T. Sasaki, K. Yasutomo, R. Hamajima, Y. Kanai, T. Kobayashi, Y. Matsuura, M. Itonaga, T. Yasui, *Sci Rep* **2022**, *12*, 1060.
[135] Y. F. Chang, W. H. Wang, Y. W. Hong, R. Y. Yuan, K. H. Chen, Y. W. Huang, P. L. Lu, Y. H. Chen, Y. M. A. Chen, L. C. Su, S. F. Wang, *Anal. Chem.* **2018**, *90*, 1861.
[136] C. Y. Lin, W. H. Wang, M. C. Li, Y. T. Lin, Z. S. Yang, A. N. Urbina, W. Assavalapsakul, A. Thitithanyanont, K. R. Chen, C. C. Kuo, Y. X. Lin, H. H. Hsiao, K. D. Lin, S. Y. Lin, Y. H. Chen, M. L. Yu, L. C. Su, S. F. Wang, *Bioeng. Transl. Med.* **2023**, *8*, e10410.
[137] A. Gupta, T. Singh, R. K. Singh, A. Tiwari, *Plasmonics* **2023**, *18*, 577.
[138] A. Kumar, P. Verma, P. Jindal, *Opt. Mater.* **2022**, *128*, 112397.
[139] G. H. Gupta, S. Kadakia, D. Agiwal, T. Keshari, S. Kumar, *Mater. Adv.* **2024**, *5*, 1803.
[140] P. K. Sharma, A. Ruotolo, R. Khan, Y. K. Mishra, N. K. Kaushik, N. Y. Kim, A. K. Kaushik, *Mater. Lett.* **2022**, *308*, 131089.
[141] V. Sorathiya, U. Soni, V. Vekariya, J. Golani, A. H. M. Almawgani, A. R. H. Alhawari, *Plasmonics* **2023**, *19*, 1211.
[142] R. Luo, J. Li, G. Huang, G. Li, S. Guo, Y. Yuan, *Microchem. J.* **2024**, *199*, 109927.

[143] M. H. M. E. Alves, L. C. Mahnke, T. C. Macedo, T. K. S. Silva, L. B. Carvalho Junior, *Biochimie* **2022**, *197*, 38.
[144] G. Moreira, L. C. Hartmann, S. P. A. Datta, D. Dean, E. McLamore, D. Vanegas, *Front. Sens.* **2022**, *3*, 917380.
[145] J. H. Lee, Y. Lee, S. K. Lee, J. Kim, C. S. Lee, N. H. Kim, H. G. Kim, *Biosensors and Bioelectronics* **2022**, *203*, 114034.
[146] J. Hou, X. Qian, Y. Xu, Z. Guo, B. Thierry, C. T. Yang, X. Zhou, C. Mao, *Biosensors and Bioelectronics* **2023**, *237*, 115423.
[147] Y. Yue, H. Ding, C. Chen, *J. Biophotonics* **2021**, *14*, e202000338.
[148] D. Kawasaki, H. Yamada, K. Sueyoshi, H. Hisamoto, T. Endo, *Biosensors* **2022**, *12*, 200.

A. Tsalsabila[ʃʃ], V. A. Dabur[ʃʃ], I. J. Budiarso, S. Wustoni, H. C. Chen, M. D. Birowosuto, A. Wibowo*, and S. Zeng*

Progress and Outlooks in Designing Photonic Biosensor for Virus Detection

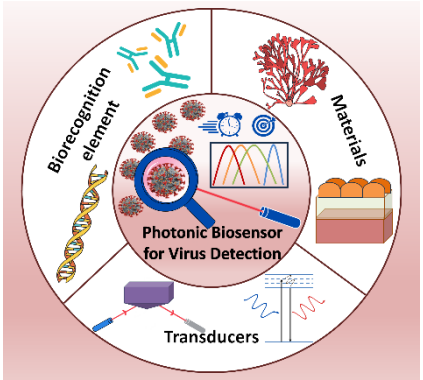

Photonic biosensors stand out as promising tools for virus detection, offering high sensitivity, selectivity, rapid monitoring, and potential for point-of-care applications. This paper presents a comprehensive overview of photonic biosensors tailored for virus detection, focusing on sensing transducers, material design, and surface functionalization strategies to enhance the biorecognition of virus detection.